

Ludwig-Maximilians-Universität München

Sektion Physik

*Flavour Independent
Search for the Higgs Boson
in the hZ Channel at LEP*

Nicole Paula Heidelies Nesvadba

Diplomarbeit – Diploma Thesis

15. Mai 2001

Erstgutachterin: Prof. Dr. Dorothee Schaile,
Zweitgutachter: Prof. Dr. Harald Fritsch

Ludwig-Maximilians-Universität München

Sektion Physik

*Flavour Independent
Search for the Higgs Boson
in the hZ Channel at LEP*

Nicole Paula Heidelies Nesvadba

Diplomarbeit – Diploma Thesis

15. Mai 2001

Abstract

A kinematic search for an electrically neutral massive scalar boson is presented. This refers especially to the light scalar Higgs boson within an extension of the Standard Model Higgs mechanism, the Two Higgs Doublet Models. It is assumed that the boson is produced by Higgs-strahlung and decays hadronically with a four jet topology. No explicit bottom quark information is used, but mass hypotheses are made between 60 and 115 GeV. Approximately 210 pb^{-1} of data are analysed with center of mass energies above 200 GeV. This is the full data that was taken in the year 2000 with the OPAL detector at the LEP storage ring at CERN. No Higgs boson was found with these studies, but limits could be set for various scenarios within Two Higgs Doublet Models and within theories where the Higgs boson is a composite of fundamental particles.

Contents

| | | |
|----------|--|-----------|
| 1 | Introduction | 1 |
| 2 | Masses in the Standard Model and Beyond | 3 |
| 2.1 | The Standard Model of Elementary Particles | 3 |
| 2.1.1 | Gauge Invariance and Electroweak Interactions | 5 |
| 2.2 | The Higgs Mechanism in the Standard Model | 8 |
| 2.2.1 | Sponaneous Symmetry Breaking and the Generation of Boson Masses | 8 |
| 2.2.2 | The Masses of Fermions | 10 |
| 2.3 | Extended Higgs Models | 11 |
| 2.3.1 | General Two Higgs Doublet Models | 12 |
| 2.3.2 | Composite Models | 13 |
| 2.4 | Constraints on the Higgs Mass | 14 |
| 2.4.1 | Theoretical Constraints | 14 |
| 2.4.2 | Experimental Limits | 16 |
| 3 | Features of a Higgs Search at LEP200 | 19 |
| 3.1 | Simulating Particle Interactions | 22 |
| 3.1.1 | Parton Showers and Hadronisation Schemes | 22 |
| 3.2 | Standard Model Interactions at 200 GeV | 24 |
| 3.2.1 | The Two Fermion Background | 24 |
| 3.2.2 | The Four Fermion Background | 25 |
| 3.3 | Properties of Neutral Higgs Decays | 28 |
| 4 | The Experimental Requirements | 29 |
| 4.1 | The OPAL Detector | 31 |
| 4.1.1 | The Inner Tracking System | 31 |
| 4.1.2 | The Calorimeters | 35 |
| 4.1.3 | The Muon Chambers | 35 |
| 4.2 | The OPAL Trigger | 36 |
| 4.3 | Correction for Double Counting | 36 |
| 4.4 | Data Samples of this Analysis | 37 |

| | | |
|----------|---|-----------|
| 5 | The Analysis Method | 39 |
| 5.1 | Elements of a Higgs Search beyond 200 GeV | 39 |
| 5.1.1 | Identifying Jets | 39 |
| 5.1.2 | Kinematic Fits | 40 |
| 5.1.3 | Matrix Elements | 42 |
| 5.2 | The Preselection | 43 |
| 5.2.1 | Variables in the Preselection | 43 |
| 5.3 | The Likelihood Selection | 45 |
| 5.3.1 | The Likelihood Ratio Method | 45 |
| 5.3.2 | Likelihood Variables | 45 |
| 5.3.3 | Figure of Merit | 46 |
| 5.3.4 | The Likelihood Cut | 47 |
| 6 | Results of the Analysis | 49 |
| 7 | Uncertainties and Systematics | 63 |
| 7.1 | Sources of Systematic Uncertainties | 63 |
| 7.1.1 | Monte Carlo Dependence | 63 |
| 7.1.2 | Different Center of Mass Energies | 64 |
| 7.1.3 | Test Mass Assumptions | 65 |
| 7.1.4 | Mismodelling of the Variables | 65 |
| 7.2 | Final Errors | 66 |
| 8 | Interpreting the Results | 67 |
| 8.1 | Deriving a Limit | 67 |
| 8.2 | General Flavour Independent Limits | 70 |
| 8.3 | Limits within 2HD Models | 70 |
| 8.4 | Combining the OPAL Channels | 71 |
| 8.5 | Limits for a Composite Higgs Boson | 76 |
| 9 | Summary and Outlook | 81 |
| A | List of Monte Carlo Simulations | 85 |

List of Figures

| | | |
|-----|---|----|
| 2.1 | Allowed mass range of the Higgs boson so that the Standard Model remains valid up to the Planck scale. | 15 |
| 2.2 | Indirect experimental limits to the Higgs mass | 17 |
| 3.1 | The Higgs-strahlung process. | 19 |
| 3.2 | The two decay modes of a Higgs boson considered in this analysis. | 20 |
| 3.3 | The cross sections for Higgs-strahlung in comparison to Standard Model processes. | 21 |
| 3.4 | $q\bar{q}$ production with gluon radiation. | 25 |
| 3.5 | Feynman diagrams of some of the possible four fermion final states | 26 |
| 3.6 | Contributions from Standard Model processes at LEP2 energies. | 27 |
| 4.1 | The LEP storage ring and the chain of accelerators used before the injection into the main ring. | 30 |
| 4.2 | The Omni Purpose Apparatus for LEP (OPAL) and its subsystems | 32 |
| 4.3 | A candidate that was selected with this analysis | 33 |
| 4.4 | Energy distribution of the year 2000 data. | 38 |
| 6.1 | The energy difference of the highest and the lowest energetic jet. | 51 |
| 6.2 | The likelihood variables for Higgs bosons with decays as in the Standard Model. | 53 |
| 6.3 | Likelihood input variables for Standard Model decays with a test mass of 110 GeV. | 54 |
| 6.4 | Likelihood input variables for the Higgs boson decaying into gluon pairs. The Higgs mass is assumed to be 60 GeV. | 55 |
| 6.5 | Likelihood input variables for a gluon final state of the Higgs boson, assuming a Higgs mass of 110 GeV. | 56 |
| 6.6 | The "number of tracks" variable for gluon and for quark final states. | 57 |

| | | |
|------|---|----|
| 6.7 | Likelihood distributions for hypothetical Higgs boson masses between 60 and 115 GeV. | 58 |
| 6.8 | Likelihood distributions for the same test masses as before, but using the reference histograms as obtained by the $h \rightarrow gg$ samples | 59 |
| 6.9 | Efficiency of the likelihood selection as a function of m_H determined from different Monte Carlo samples. | 60 |
| 6.10 | The number of events recorded in the year 2000 that pass the likelihood selection for test masses between 60 GeV and 115 GeV. | 61 |
| 8.1 | $1 - CL_B$ is given for a range of test masses between 80 and 115 GeV. | 69 |
| 8.2 | The excluded cross sections with respect to the Standard Model Higgs boson versus Higgs masses between 80 GeV and the kinematic limit. | 72 |
| 8.3 | Standard Model cross sections and minimal branching fractions for Higgs-strahlung in 2HDM. | 73 |
| 8.4 | The expected limit (green line) and the observed limit (red line), accounting for the minimal production cross section in 2HD models. | 74 |
| 8.5 | Limits obtained by combining the flavor independent OPAL search channels. | 75 |
| 8.6 | Exclusion limits on a 95 % Confidence Level if only Higgs boson decays into gluons are considered. | 78 |
| 8.7 | Cross section limits for a composite Higgs boson that decays predominantly into gluons. | 79 |

List of Tables

| | | |
|-----|---|----|
| 2.1 | The twelve known fundamental fermions and some of their properties. | 4 |
| 2.2 | The known fundamental bosons and the hypothetical neutral Higgs boson. | 4 |
| 6.1 | Cutflow table for an assumed mass of the Higgs boson of 100 GeV. | 50 |
| 7.1 | The errors that were obtained when using alternative Monte Carlo Simulations. | 64 |
| 7.2 | The center of mass energy of the year 2000 data, given in bins of 2 GeV around the indicated values. | 64 |
| 7.3 | Uncertainties due to mismodelling of the variables in the Monte Carlo event generators. | 65 |
| 7.4 | Overview of the systematic errors in the background estimation as obtained with the above procedures. | 66 |
| 7.5 | The considered systematic errors of the efficiency as obtained for the Standard Model Higgs samples. | 66 |
| 8.1 | Branching fractions for a composite Higgs boson | 76 |

Chapter 1

Introduction

Do people worry about physics? Not really. But if one did a survey on what they know about it, a frequent answer could be:

$$E = mc^2 \tag{1.1}$$

Three letters, one number. How many people know what these letters stand for? Probably very few. The energy E – an everyday, but quite abstract quantity, well defined only in physics. The speed of light, c . A huge number, and its square is even bigger. By far too big to be a useful measure on Earth. The only everyday element in Einstein’s famous formula is the mass m . Everybody can easily estimate how much is a kilogram, or at least a pound. Mass is something one can be sure upon. Except if one is a physicist.

What is mass? That question does not only nowadays puzzle physicists’ minds. Classical mechanics knows even about two masses: the heavy mass of gravity

$$\vec{F} = g \frac{m_1 m_2}{r^3} \vec{r} \tag{1.2}$$

and the inert mass of Newton’s second axiom:

$$\vec{F} = m \frac{d^2 \vec{r}}{dt^2} \tag{1.3}$$

In 1915 Albert Einstein *defined* both to be equal, without giving an explanation – the equivalence principle is one of the foundations of General Relativity. And today particle physicists just admit that they don’t know ... yet. But they keep on working. And they have an idea: the Higgs Mechanism.

Most of the mass in the universe – as far as it can be seen – in fact is already unmasked. As one looks at the smaller and smaller components of matter, it becomes evident that the biggest part of ”mass” is on the microscopic scale ”binding energy”, a result of the attractive potential between

the quarks. Only a tiny fraction (around 1 part per mille) of for example the proton mass comes from its constituent quarks.

A tiny fraction, and a big problem. Because in the very well established and scrutinized Standard Model of elementary particle physics, all particles are massless. This is even a requirement, since the basic structure of the theory, the "gauge invariance", is lost if one just adds terms for the particle masses "by hand". The problem became more evident in 1983, when scientists at the European Particle Physics Center CERN discovered the three gauge bosons W^\pm and Z^0 . They have masses of approximately 80 and 90 GeV, respectively. That is roughly equivalent to the nucleus of a silver atom. These masses are large compared to the 1 GeV mass of a proton. And this time binding energy does not provide a way out, because in the Standard Model the gauge bosons are not bound states, but fundamental particles. Yet they could yield the key to the mass problem.

The gauge bosons emerge as resonant states of relativistic quantum fields, the so-called electroweak gauge fields. These fields were predicted by Glashow, Salam and Weinberg in the sixties, when they found that two of the four fundamental forces – the electromagnetic and the weak interaction – are just two different aspects of the same underlying structure. This electroweak interaction requires additional fields – the gauge fields – and the ultimate proof for the existence of electroweak gauge fields are the gauge bosons.

It is the special structure of the electroweak interaction that could also yield the masses – at least the masses of the electroweak bosons, if not particle masses in general. But just adding a standard mass term is forbidden. Therefore a dynamical mechanism is needed to obtain particle masses: the "Higgs Mechanism". It is elegant but rather arbitrary as some people object. At present it is the only seriously discussed option. Its basic concept, "Spontaneous Symmetry Breaking", at least has been observed in other branches of physics.

The Higgs mechanism requires the existence of one more field, the Higgs field. As in the case of the gauge bosons, the existence of this field must be proven via the discovery of at least one more particle: the Higgs boson. Particle physicists search for Higgs bosons in international collaborations in Switzerland (CERN) as well as in the United States (Fermi National Accelerator Laboratory). So far, no definite signature of the Higgs boson has been found, even though there were some hints for an observation last autumn. This thesis presents a search for the Higgs boson. It was performed at the OPAL experiment, one of the detectors at CERN's Large Electron Positron collider LEP. It did not lead to a discovery, but helped to rule out parts of the parameter space in different Higgs models.

Chapter 2

Masses in the Standard Model and Beyond

2.1 The Standard Model of Elementary Particles

The Standard Model [1, 2, 3, 4] today is one of the experimentally best tested theories in physics. It describes the fundamental quanta (particles) and their interactions except for gravity at an energy scale of up to a few hundred GeV. This is done in the framework of gauge theory, by respecting the conservation laws resulting from a $SU(3) \times SU(2) \times U(1)$ symmetry.

Two classes of particles can be distinguished: fermions and bosons. Fermions are believed to be the fundamental constituents of matter. Twelve different fermions are known - six quarks and six leptons. Both groups can be further separated into three "generations" with two members each (table 2.1). Corresponding members of different generations carry the same quantum numbers, but they differ in mass. Within the Standard Model this pattern cannot be deduced from first principles and neither can the number of generations be explained. Experimentally and in the today accessible energy range, the latter was confirmed to high precision with the measurements at the LEP collider [5].

Three types of forces act between the fermions, if the momentum transfer remains small: the *strong*, the *electromagnetic* and the *weak* interaction. Theorists believe that these interactions will unify if the energy of the interaction rises to about 10^{16} GeV. At energies of a few 100 GeV, this is already true for the electromagnetic and the weak force (c. f. 2.1.1). This *electroweak* interaction unifies all phenomena of electromagnetic and weak processes in a single $SU(2) \times U(1)$ symmetry. In the limit of a vanishing momentum transfer, its equations yield the separate descriptions of electromagnetic processes (in agreement with Quantum Electrodynamics [6]) and of weak interactions, as given in Fermi's Theory for β and muon decay [7].

| | mass [GeV] | spin | el. charge |
|-------------------|-----------------|------|------------|
| up | 0.001 - 0.005 | 1/2 | +2/3 |
| down | 0.003 - 0.009 | 1/2 | -1/3 |
| charm | 1.150 - 3.500 | 1/2 | +2/3 |
| strange | 0.075 - 0.17 | 1/2 | -1/3 |
| top | 174.3 ± 5.1 | 1/2 | +2/3 |
| bottom | 4 - 4.4 | 1/2 | -1/3 |
| electron | 0.511 MeV | 1/2 | -1 |
| electron neutrino | < 3 eV | 1/2 | 0 |
| muon | 105.66 MeV | 1/2 | -1 |
| muon neutrino | < 0.19 MeV | 1/2 | 0 |
| tau | 1777.03 MeV | 1/2 | -1 |
| tau neutrino | < 18.2 MeV | 1/2 | 0 |

Table 2.1: In the upper half the six quarks, the leptons are shown below. Their properties will be further explained in the text.

| | mass | spin | el. charge |
|---------|-----------------------------|------|------------|
| gluon | < $\mathcal{O}(\text{MeV})$ | 1 | 0 |
| photon | < $2 \cdot 10^{-16}$ eV | 1 | 0 |
| Z^0 | 91,186 - 91,19 GeV | 1 | 0 |
| W^\pm | 80,363 - 80.475 GeV | 1 | ± 1 |
| Higgs | > 113.5 GeV | 0 | 0 |

Table 2.2: The known fundamental bosons and the hypothetical neutral Higgs boson. The properties will be further explained in the text.

All types of interactions are mediated by a second class of particles, the bosons. Fermions and bosons differ in their spin and therefore in their quantum statistics. Whereas the fundamental fermions are all spin-1/2 particles, bosons carry integer spin (table 2.2).

The strong force is described by Quantum Chromodynamics (QCD) which operates on quarks and gluons. Only those particles carry the corresponding $SU(3)$ charge, called color. Each quark carries one color. If the three colors are present in a bound state of quarks, then the resulting object is color neutral.

Gluons are the mediators of the strong force. They carry a non-vanishing combination of a color and an anticolor, therefore they interact with themselves.

One of the predominant features of QCD is "asymptotic freedom". Perturbative calculations (see chapter 2.1.1) can be applied only for high mo-

momentum transfers, because the strong coupling constant increases with decreasing energy. The color degrees of freedom are "confined" at low energies: Only color singlet composites of quarks, such as mesons (quark and anti-quark with opposite color) or baryons (three quarks of different color) can exist. This is in good agreement with experiment: free quarks have never been observed [8].

2.1.1 Gauge Invariance and Electroweak Interactions

As was stated by Glashow, Salam and Weinberg during the 1960s [1, 2, 3], an adequate description of particle processes up to energies of some 100 GeV can be given if weak and electromagnetic interactions are two aspects of the same symmetry, thus leading to a simultaneous consideration of $SU(2)_L \times U(1)_Y$, with the *weak isospin* and the *hypercharge* as generators (see equation 2.7).

In Quantum Field Theory the dynamic of a state is governed by its Lagrange density or *Lagrangian* \mathcal{L} . Of course this also applies to the Standard Model. The Lagrangian has to embody a number of postulates and it will be shown how they lead to the prediction of the physically observed electroweak gauge bosons. Here we limit the formalism to leptons, as the procedure for quarks is mathematically more involved. It can be found for example in [9, 10, 11].

Local Gauge Invariance

It is required that transformations of the gauge fields under a symmetry group must leave the Lagrangian unchanged. Unlike in *global* gauge invariance, in *local* gauge transformations the phase is a function of the space-time coordinates. An example is the transformation under $U(1)$:

$$\psi \rightarrow \psi' = \psi \exp[igY(x)], \quad (2.1)$$

with the phase $gY(x)$. Y is the generator of the group, and g the coupling constant, a real number.

The Electroweak Lagrangian for Massless Particles

The simplified Lagrangian describing the electroweak interactions of massless particles is given by

$$\mathcal{L}_{ew} = -\frac{1}{4}G_{\mu\nu}G^{\mu\nu} - \frac{1}{4}F_{\mu\nu}F^{\mu\nu} + \bar{\Psi}i\gamma_\mu D^\mu\Psi, \quad (2.2)$$

The first two terms concern the gauge fields: namely the tensor $G_{\mu\nu}$ yields the $SU(2)_L$ gauge fields W_μ , and the tensor $F_{\mu\nu}$ yields the $U(1)_Y$ gauge fields B_μ . Y indicates the hypercharge. The last term describes the interaction of fermions with the gauge fields. D^μ is the covariant derivative, γ_μ are the usual γ matrices and Ψ represents the fermion wave function.

The index L is given because only left handed fermions participate in the weak interaction. This is a consequence of the explicit parity violation in electroweak interactions. Thus they are put into the fundamental representation of $SU(2)$, in other words they form the left handed *weak isospin doublets* L :

$$L = \frac{1}{2}(1 - \gamma_5) \begin{pmatrix} \nu_e \\ e \end{pmatrix} = \begin{pmatrix} \nu_e \\ e \end{pmatrix}_L. \quad (2.3)$$

Right handed fermions are introduced into the theory as the isospin singlets e_R and ν_R . Right handed neutrinos have never been observed [8].

These different roles of left and right handed fermions in the interaction must formally be accounted for by introducing two different covariant derivatives:

$$\begin{aligned} D_L^\mu &= \partial^\mu + i\frac{g}{2}(\tau W^\mu) + i\frac{g'}{2}B^\mu Y_L, \\ D_R^\mu &= \partial^\mu + i\frac{g'}{2}B^\mu Y_R \end{aligned} \quad (2.4)$$

The first line gives the derivative for left handed particles, the second line refers to the right handed leptons. The electroweak hypercharge is also different for both particle types: $Y_L = -1$, while $Y_R = -2$. g and g' represent the coupling constants of the W^μ and the B^μ fields, respectively. τ indicates the Pauli matrices.

The electroweak Lagrangian can then be written as the sum of two terms: a purely kinetic term \mathcal{L}_{kin} and an interaction term \mathcal{L}_{int} such that $\mathcal{L} = \mathcal{L}_{kin} + \mathcal{L}_{int}$, where the kinetic term is given by

$$\mathcal{L}_{kin} = i\bar{L}\gamma_\mu\partial^\mu L - i\bar{\nu}_{eR}\gamma_\mu\partial^\mu\nu_{eR} + i\bar{e}_R\gamma_\mu\partial^\mu e_R, \quad (2.5)$$

and the interaction term by

$$\begin{aligned} \mathcal{L}_{int} &= \frac{g}{\sqrt{2}}\bar{L}\gamma^\mu\tau^+LW_\mu^+ + \frac{g}{\sqrt{2}}\bar{L}\gamma^\mu\tau^-LW_\mu^- \\ &+ \frac{g}{2}W_3^\mu(\bar{\nu}_{eL}\gamma_\mu\nu_{eL} - \bar{e}_L\gamma_\mu e_L) \\ &+ \frac{g'}{2}B^\mu[Y_L(\bar{\nu}_{eL}\gamma_\mu\nu_{eL} + \bar{e}_L\gamma_\mu e_L) + Y_{\nu_{eR}}\bar{\nu}_{eR}\gamma_\mu\nu_{eR} + Y_{e_R}\bar{e}_R\gamma_\mu e_R] \end{aligned} \quad (2.6)$$

with $\tau^\pm = \frac{1}{2}(\tau_1 \pm \tau_2)$. The interactions as described by the first line differ physically from those in the second and third line, as the former carry electric charge. Therefore they are called *charged currents*. This is indicated by the indices \pm . These charged currents emerge as a combination of the first two components of the gauge field W_μ : $W_\mu^\pm = \frac{1}{\sqrt{2}}(W_\mu^1 \mp iW_\mu^2)$. Interactions

with the third component W_μ^3 and with the B_μ field are electrically neutral. Therefore they are referred to as *neutral currents*.

In order to finally obtain the electroweak theory, one must account explicitly for the electromagnetic vector field A_μ . This can be done using the relation between the electric charge Q , the weak hypercharge and the third component of the weak isospin:

$$Q = \frac{Y}{2} + T_3 \quad (2.7)$$

with the hypercharge Y and the third component of the weak isospin T_3 . To assure an electromagnetic interaction which does not couple to the neutrinos, a rotation must be done in the space of the neutral gauge fields B_μ and W_μ^3 that introduces the fields Z_μ and A_μ :

$$B_\mu = A_\mu \cos \theta_W - Z_\mu \sin \theta_W \quad (2.8)$$

$$W_\mu^3 = A_\mu \sin \theta_W + Z_\mu \cos \theta_W \quad (2.9)$$

with the weak mixing angle θ_W . The neutral terms of the Lagrangian then take the form:

$$\begin{aligned} \mathcal{L}_n^W &= \bar{\Psi} \gamma_\mu (g \sin \theta_W T_3 + g' \cos \theta_W \frac{Y}{2}) \Psi A_\mu \\ &+ \bar{\Psi} \gamma_\mu (g \cos \theta_W T_3 - g' \sin \theta_W \frac{Y}{2}) \Psi Z_\mu \end{aligned} \quad (2.10)$$

With the above definition of the weak hypercharge Y and the electron charge $e = g \sin \theta_W$ it can be shown that A_μ couples to the electromagnetic current

$$J_{em}^\mu = -e(\bar{e}_R \gamma^\mu e_R + \bar{e}_L \gamma^\mu e_L) \equiv e \bar{\Psi} \gamma^\mu Q \Psi, \quad (2.11)$$

the electromagnetic charge Q is given in units of the positron charge.

Hence, the two gauge fields W_μ and B_μ finally lead to four physical bosons. W_μ yields the two charged electroweak gauge bosons W^+ and W^- by

$$W_\mu^\pm = \frac{W_\mu^1 \mp i W_\mu^2}{\sqrt{2}}. \quad (2.12)$$

Its third component mixes with the field B_μ , resulting in a neutral electroweak gauge boson, the Z^0 , corresponding to

$$Z_\mu = \frac{-g' B_\mu + g W_\mu^3}{\sqrt{g^2 + g'^2}}. \quad (2.13)$$

The fourth boson is the photon γ , corresponding to the A_μ field:

$$A_\mu = \frac{g}{\sqrt{g^2 + g'^2}} B_\mu + \frac{g'}{\sqrt{g^2 + g'^2}} W_\mu^3 \quad (2.14)$$

These last two equations were obtained from equations 2.8 and 2.9, setting $\sin \theta_W = \frac{g'}{\sqrt{g^2 + g'^2}}$

Renormalisation

Electroweak processes are calculated by the means of *perturbation theory*. Quantities such as cross-sections are approximated by expanding them into terms of ascending order, the actual calculations being performed only up to a finite order (usually second or third). Convergence requires that the coupling constants are sufficiently small.

Perturbative calculations break down when the terms increase with increasing orders, finally leading to infinite coupling constants or masses (loop divergences) [11, 12]. In a number of cases (e. g. QED) this can be avoided by combining infinite, but experimentally unobservable quantities in a way that the combined values – the *renormalized parameters* – remain finite. In 1971 t’Hooft and Veltman showed that the electroweak theory is renormalizable [13] (unlike the bare Fermi theory of the weak interaction), and therefore its properties can be calculated using perturbation theory.

2.2 The Higgs Mechanism in the Standard Model

At this point fermions and bosons are still massless, as the Lagrangians do not include any mass terms, in contradiction to experimental results. Mathematically though, the mere adding of mass terms to the Standard Model Lagrangian would spoil its gauge invariance, because mass terms (for example $M^2 W_\mu W^\mu$ for the weak bosons) are not invariant under local gauge transformations.

The Higgs mechanism [14] provides an indirect way to attribute mass terms to particles, which is commonly referred to as *Spontaneous Symmetry Breaking*, a phenomenon that was first observed in solid state physics [15]. The masses of the electroweak bosons are given by the parameters of the mechanism. On the other hand, the Higgs mechanism fails in the quantitative prediction of fermion masses. Empirical parameters, the Yukawa couplings, must be included.

2.2.1 Spontaneous Symmetry Breaking and the Generation of Boson Masses

In a first step it will be shown how the mass terms of electroweak gauge bosons emerge as a direct consequence of the Higgs mechanism. A new field is added to the electroweak Lagrangian, the so called Higgs field, that interacts with the electroweak gauge bosons. The according Lagrangian is explicitly given by

$$\mathcal{L}_{Higgs} = (D_\mu \phi)^\dagger D^\mu \phi - \mu^2 \phi^\dagger \phi + \lambda (\phi^\dagger \phi)^2 \quad (2.15)$$

ϕ indicates the Higgs field. It is an $SU(2)$ isospin doublet

$$\phi = \begin{pmatrix} \phi^+ \\ \phi^0 \end{pmatrix} \quad (2.16)$$

that consists of the two complex scalar fields $\phi^+ = \frac{a+ib}{\sqrt{2}}$ and $\phi^0 = \frac{a'+ib'}{\sqrt{2}}$.

The covariant derivative again yields the kinetic term, while the remaining parts describe a potential:

$$V = \mu^2 \phi^\dagger \phi - \lambda (\phi^\dagger \phi)^2, \quad (2.17)$$

μ^2 and λ being two real scalar parameters. λ should be chosen to be positive, otherwise the potential will not be bound from below. This Lagrangian is of the most general renormalizable form [12].

The potential V yields the key to the Higgs mechanism. The ground state can be given in a unique way only when it is not degenerate. Otherwise, one ground state must be chosen arbitrarily – *spontaneously* – out of the set of degenerate states. This ground state therefore does not necessarily have the same symmetries as the original Lagrangian. This means that mass terms can arise for the ground state while the overall symmetry of the Lagrangian is kept.

In field theory the ground state is the vacuum state. Therefore the Higgs field is assumed to have a non-vanishing constant expectation value $\langle 0|\phi(x)|0\rangle = \text{constant} \neq 0$ in the vacuum. The descriptions below follow the arguments given in [16] and [17].

Two scenarios are possible, depending on the sign of μ^2 :

- For $\mu^2 > 0$ the vacuum state will be obtained when $\phi = 0$, which is a unique ground state. Thus, there will be no spontaneous symmetry breaking in this case.
- For $\mu^2 < 0$ the vacuum state has

$$\phi^\dagger \phi = \frac{-\mu^2}{2\lambda} = \frac{v^2}{2} \quad (2.18)$$

which can be fulfilled by an infinite number of degenerate ground states, one of which is

$$\phi_0 = \frac{1}{\sqrt{2}} \begin{pmatrix} 0 \\ v \end{pmatrix} \quad (2.19)$$

This vacuum state is not invariant under general $SU(2)$ transformations.

Simultaneously, the invariance of the local $U(1)$ gauge group of the electromagnetic field must not be broken, because the photon is observed to be massless. This can be assured using the weak hypercharge (equation

2.7) and setting the hypercharge of the Higgs field to $Y = \frac{1}{2}$. Then the lower component of the Higgs doublet will be electrically neutral and the spontaneous symmetry breaking does not affect electromagnetic charge conservation in the Higgs boson interactions [16].

The spectrum of the system can now be calculated by expanding around the vacuum state, setting

$$\phi(x) = \frac{1}{\sqrt{2}} \begin{pmatrix} 0 \\ v + h(x) \end{pmatrix}, \quad (2.20)$$

the expansion being carried out around $h(x) = 0$. This finally leads to the Lagrangian (setting $Y = 1$):

$$\begin{aligned} \mathcal{L} = & \frac{1}{2}(\partial_\mu h)(\partial^\mu h) - \\ & - \lambda v^2 h^2 - \lambda v h^3 - \frac{\lambda}{4} h^4 + \\ & + \frac{1}{8} v^2 g^2 ((W_\mu^1)^2 + (W_\mu^2)^2) + \frac{1}{8} v^2 (g' B_\mu - g W_\mu^3)^2 \end{aligned} \quad (2.21)$$

This Lagrangian describes a new particle, the *Higgs boson*, together with its self interaction terms (first two lines) and its interaction with the W_μ and the B_μ vector fields (last line). These last two terms can be regarded as mass terms for the physical W and the Z bosons.

Comparing the general form of a mass term for W^\pm bosons (where the mass m is introduced as $m^2 W^+ W^-$) with equation 2.12 shows that the Higgs Mechanism leads to a W^\pm boson with a mass of

$$M_W = \frac{vg}{2}, \quad (2.22)$$

comparison with equation 2.13 leads to

$$M_Z = \frac{1}{2} v \sqrt{g'^2 + g^2}, \quad (2.23)$$

for the mass of a Z boson.

For the A_μ field (equation 2.14) no term arises in the Higgs Lagrangian. Therefore the photon mass is given by

$$M_\gamma = 0, \quad (2.24)$$

so that the photon is a massless particle.

2.2.2 The Masses of Fermions

Only the electroweak gauge bosons have acquired mass at this point, while the fermions are still massless. The Higgs mechanism can in principle cure this

in a similar manner, but coupling parameters must be introduced, so that the theoretically derived fermion masses can be adjusted to the measured values. These yield the strength of the interaction of a fermion with the Higgs field and thus determine the fermion's mass.

The procedure will be shown for leptons. The following Lagrangian is introduced to describe the interaction between leptons and the Higgs field:

$$\mathcal{L}_{Yuk} = g_e(\bar{L}\phi e_R + \phi^\dagger \bar{e}_R L) \quad (2.25)$$

where g_e is an arbitrary real coupling parameter. Expanding the Higgs field as in the previous section leads to

$$\begin{aligned} \mathcal{L}_{Yuk} &= \frac{g_e v}{\sqrt{2}}(\bar{e}_L e_R + \bar{e}_R e_L) + \frac{g_e}{\sqrt{2}}(\bar{e}_L e_R + \bar{e}_R e_L)H \\ &= m_e \bar{e}e + \frac{m_e}{v} \bar{e}eH, \end{aligned} \quad (2.26)$$

thus leading to a fermion mass of the form

$$m_e = g_e \frac{v}{2} \quad (2.27)$$

The *Yukawa couplings* g_e are arbitrary parameters that must be tuned to the measured fermion masses.

2.3 Extended Higgs Models

Up to now, there is no experimental evidence for the Higgs Mechanism as discussed above. Even though this "minimal" Higgs Mechanism is the one with the easiest mathematical structure, there exist a number of more complex approaches that are in agreement with the Standard Model.

Extensions of the Standard Model which remain valid at higher energy scales even require an extended Higgs Mechanism. They are constrained by several experimental facts. One of them is the ratio ρ of the masses of the W and the Z bosons and the electroweak mixing angle θ_W [18]:

$$\rho = \frac{m_W^2}{m_Z^2 \cos^2 \theta_W} \quad (2.28)$$

Measurements show that this value is very close to 1 [8]. While the minimal Higgs model automatically satisfies this requirement, this is not the case in most of the more complex theories. The number of Higgs doublets is especially constraint by precision measurements of ρ .

Another constraint comes from the observation that Flavour Changing Neutral Currents (FCNC) are strongly suppressed [8]. While this is automatically the case in the minimal Higgs Mechanism, this imposes further constraints on more general models. Following a theorem by Glashow and Weinberg [19], FCNCs are suppressed only when all fermions of a given electric charge do not couple to more than one Higgs doublet.

2.3.1 General Two Higgs Doublet Models

One class of models fulfills all the above requirements, which are the Two Higgs Doublet Models (2HDM) The discussion follows [18]. Instead of only one electroweak Higgs doublet there are two

$$\phi_1 = \begin{pmatrix} \phi_1^0 \\ \phi_1^- \end{pmatrix}, \phi_2 = \begin{pmatrix} \phi_2^+ \\ \phi_2^0 \end{pmatrix}, \quad (2.29)$$

leading to a much broader phenomenological spectrum than in the minimal model.

The most general potential involving two Higgs doublets that respects gauge invariance and conserves $U(1)$ is

$$\begin{aligned} V(\phi_1, \phi_2) = & \lambda_1(\phi_1^\dagger \phi_1 - v_1^2)^2 + \lambda_2(\phi_2^\dagger \phi_2 - v_2^2)^2 \\ & + \lambda_3[(\phi_1^\dagger \phi_1 - v_1^2) + (\phi_2^\dagger \phi_2 - v_2^2)]^2 \\ & + \lambda_4[(\phi_1^\dagger \phi_1)(\phi_2^\dagger \phi_2) - (\phi_1^\dagger \phi_2)(\phi_2^\dagger \phi_1)] \\ & + \lambda_5[\text{Re}(\phi_1^\dagger \phi_2) - v_1 v_2]^2 + \lambda_6[\text{Im}(\phi_1^\dagger \phi_2)]^2 \end{aligned} \quad (2.30)$$

It can be shown that this leads to two vacuum expectation values for the fields ϕ_1 and ϕ_2 , in analogy to the minimal mechanism, with

$$\langle \phi_1 \rangle = \begin{pmatrix} 0 \\ v_1 \end{pmatrix}, \quad (2.31)$$

$$\langle \phi_2 \rangle = \begin{pmatrix} 0 \\ v_2 \end{pmatrix}, \quad (2.32)$$

if all the parameters λ_i are real and not negative.

As before, the non-zero vacuum expectation values break the $SU(2) \times U(1)$ symmetry of the Lagrangian and lead to mass terms for the W and Z bosons. Instead of only one massive Higgs boson, the 2HDM lead to a total of five particles: two charged Higgs bosons H^\pm , the neutral CP-odd A^0 , the light CP-even scalar h^0 and the heavy CP-even scalar H^0 . Their properties depend on the ratio of the two vacuum expectation values:

$$\tan \beta = \frac{v_2}{v_1}. \quad (2.33)$$

The boson masses are given by

$$m_{H^\pm}^2 = \lambda_4(v_1^2 + v_2^2), \quad (2.34)$$

$$m_{A^0}^2 = \lambda_6(v_1^2 + v_2^2), \quad (2.35)$$

$$m_{H^0, h^0}^2 = 0.5[\mathcal{M}_{11} + \mathcal{M}_{22} \pm \sqrt{(\mathcal{M}_{11} - \mathcal{M}_{22})^2 + 4\mathcal{M}_{12}^2}]. \quad (2.36)$$

where H^0 and h^0 mix through the matrix \mathcal{M} as given by

$$\mathcal{M} = \begin{pmatrix} 4v_1^2(\lambda_1 + \lambda_3) + v_2^2\lambda_5 & (4\lambda_3 + \lambda_5)v_1v_2 \\ (4\lambda_3 + \lambda_5)v_1v_2 & 4v_2^2(\lambda_2 + \lambda_3) + v_1^2\lambda_5 \end{pmatrix} \quad (2.37)$$

or in terms of a mixing angle α :

$$\sin 2\alpha = \frac{2\mathcal{M}_{12}}{\sqrt{(\mathcal{M}_{11} - \mathcal{M}_{22})^2 + 4\mathcal{M}_{12}^2}} \quad (2.38)$$

$$\cos 2\alpha = \frac{\mathcal{M}_{11} - \mathcal{M}_{22}}{\sqrt{(\mathcal{M}_{11} - \mathcal{M}_{22})^2 + 4\mathcal{M}_{12}^2}}, \quad (2.39)$$

Then the five Higgs bosons are given in terms of α and β as:

$$H^\pm = -\phi_1^\pm \sin \beta + \phi_2^\pm \cos \beta \quad (2.40)$$

$$A^0 = \sqrt{2}(-Im\phi_1^0 \sin \beta + Im\phi_2^0 \cos \beta) \quad (2.41)$$

$$H^0 = \sqrt{2}[(Re\phi_1^0 - v_1) \cos \alpha + (Re\phi_2^0 - v_2) \sin \alpha] \quad (2.42)$$

$$h^0 = \sqrt{2}[-(Re\phi_1^0 - v_1) \sin \alpha + (Re\phi_2^0 - v_2) \cos \alpha], \quad (2.43)$$

In agreement with the Glashow-Weinberg theorem two different types of Higgs-fermion interaction are possible within the 2HDM:

1. Type I:

- ϕ_1 does not couple to fermions at all,
- ϕ_2 yielding the Standard Model couplings

2. Type II:

- ϕ_1 couples exclusively to up type fermions with charge $+2/3$,
- ϕ_2 couples exclusively to down type fermions with charge $-1/3$ ¹

2.3.2 Composite Models

2HD models presently are a popular way to extend the Minimal Higgs Model, not the least because they are a necessary ingredient of Supersymmetry [18], one of the favoured approaches reaching beyond the Standard Model. There exist alternative theories though which predict Higgs bosons with masses in a similar range. One of them is the interpretation of electroweak interactions as a confinement phenomenon [20].

In this model, the electroweak bosons are considered as bound states of fundamental scalar Higgs bosons [21]. Their angular momenta can either add to a total value of $J = 1$ or $J = 0$, as known e. g. for the hydrogen atom. Three different configurations can lead to the state with $J = 1$, which are

¹In the following, “2HDM” will always refer to type II models, if not explicitly stated otherwise.

the vector particles: the W^+ boson (hh), the W^- boson (hh)[†], and the Z boson ($\bar{h}h$). The $J = 0$ state ($\bar{h}h$) yields the Standard Model Higgs boson.

The Higgs couplings to the gauge bosons are the same as in the Standard Model, so the production cross sections for Higgs bosons are equal. The couplings to fermions on the contrary can be suppressed or even vanish. In this composite model only the top quark, whose mass is of the order of the gauge boson masses, is assumed to have a mass. The other quarks, being much lighter than the top, acquire a *dynamical mass* as a side effect of flavour mixing. They have mass terms in their Lagrangians but do not couple to the composite Higgs boson.

The main decay channels of the Higgs boson are into gluon pairs, photons and (above a Higgs mass of around 90 GeV) into W pairs:

$$\begin{aligned} H &\rightarrow gg \\ H &\rightarrow \gamma\gamma \\ H &\rightarrow WW \end{aligned} \tag{2.44}$$

2.4 Constraints on the Higgs Mass

In the Standard Model, the mass of the Higgs boson is given by

$$m_H = \sqrt{2\lambda}v \tag{2.45}$$

The vacuum expectation value v can be deduced from the measured value of the Fermi coupling constant as $v = (G_F\sqrt{2})^{-1} \sim 246$ GeV. The quartic Higgs coupling λ is unknown. Therefore, the Standard Model does not predict the Higgs boson mass. Only constraints can be given in order to reduce the possible mass range. Approaches have been made both from theoretical considerations and experimental results. Some features are presented here for the case of the Standard Model, as this is the best studied framework. Analogous investigations have been made for other theories as well.

2.4.1 Theoretical Constraints

A lower limit to the Higgs mass can be derived from vacuum stability [18]. By considering that the Higgs potential has been stable over a time long enough to allow the present universe to have formed, quantitative statements can be made about its shape. There is full vacuum stability if the present Higgs minimum is an absolute one. Even if this is not the case, then estimates of its value can be made which depend on the observed age of the universe. This constraint leads to a lower bound that is well below the present experimental predictions.

The upper bound of possible Higgs masses in a perturbation theory is estimated to be about 1 TeV. If the Higgs mass is too large, then processes

involving Higgs contributions will become dominant in higher order terms, causing perturbation theory to break down.

Those results can be translated into an energy cut-off up to which the Standard Model yields the correct theory. If the Standard Model remains valid up to the energy scale of Grand Unification (where all fundamental interactions including gravity are of comparable strength), then there remains an allowed range from about 130 to 190 GeV for the Higgs mass [22] (c.f. fig. 2.4.1). If the mass is outside this range, then new physics must emerge at energies between the Standard Model (100 GeV) and Grand Unification (10^{16} GeV) [23].

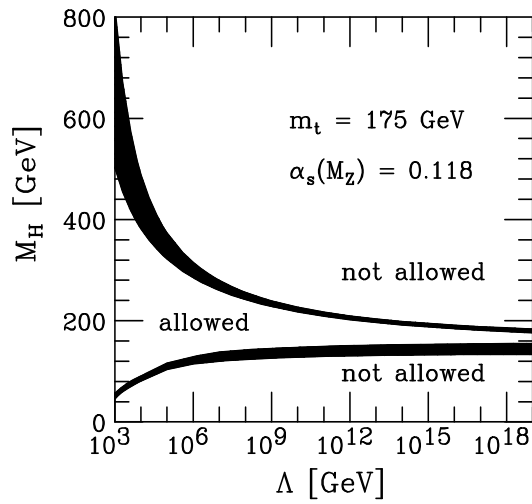


Figure 2.1: Allowed mass range for the Higgs boson so that the Standard Model remains valid up to the Planck scale [23]. The top mass is assumed to be $m_t = 175$ GeV, the strong coupling constant $\alpha_s = 0.118$. The Standard Model will break down at an energy scale below 10^{19} GeV if its mass is below 130 GeV or above 190 GeV.

2.4.2 Experimental Limits

At the end of the LEP experiments, precise measurements of the electroweak parameters set much stricter bounds to the Higgs mass than theory [24]. One such measurement is the energy dependence of the Z production that was performed at LEP in the first half of the 1990s.

The Higgs mass can further be deduced from radiative corrections involving Higgs loops. This is done with precise measurements of the W boson and the top quark masses. All approaches have not given any hint that the Standard Model Higgs boson exists, but they decrease the range of its possible mass.

The χ^2 fit of the relevant electroweak data to the Standard Model parameters shows that the Higgs boson should not have a mass exceeding 212 GeV [24] within the 95 % confidence level (upper part of figure 2.2). The lower plot shows the combined indirect measurements of the top quark and the W boson mass as obtained at LEP and the Stanford based SLD. In addition the direct measurements of the W and the top quark mass are shown. They were obtained at the Tevatron Collider of the Fermi National Accelerator Laboratory. All approaches agree for a large mass range. Hypothetical Higgs masses between 113 and 1000 GeV are indicated by the light band.

The best lower mass bound of the Standard Model Higgs boson is given by the combined results of the direct searches [25] at the four experiments of the LEP collider (c.f. chapter 4). Its present value is 113.5 GeV.

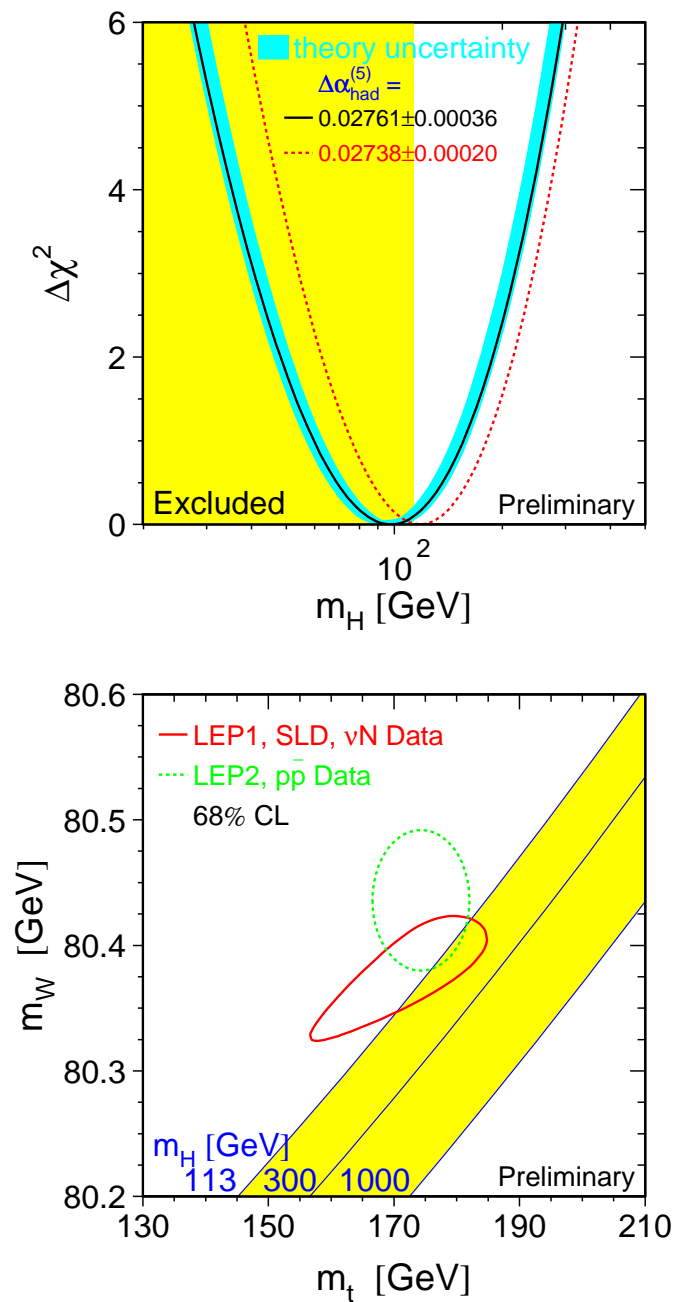


Figure 2.2: *above*: The fit of electroweak data that yields a constraint to the Higgs mass. *below*: The range of possible Higgs masses, as obtained by the measured masses of the top quark and the W boson.

Chapter 3

Features of a Higgs Search at LEP200

This analysis searches for the lightest Higgs boson within the theoretical framework of general Two Higgs Doublet Models. It is optimised for events with four quarks in the final state. The background is mainly due to W and Z pairs (“four fermion background”) as well as to quark pair production (“two fermion background”).

The Higgs boson is assumed to be produced by the Higgs-strahlung process. This is the dominant production channel for Standard Model Higgs bosons at energies within the reach of the LEP experiments. It occurs when an off shell Z boson radiates a Higgs boson and becomes on shell (Fig. 3.1). The Higgs-strahlung cross sections are shown in fig. 3.3 for a number of hypothetical Higgs masses and in comparison with some of the Standard Model processes.

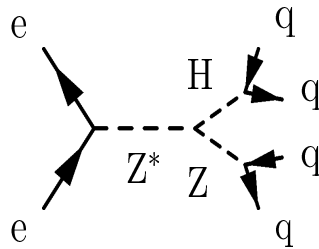


Figure 3.1: The Higgsstrahlung process. In the initial e^+e^- collision, an off shell Z boson is produced, which radiates a Higgs boson and becomes on shell. Here both bosons decay further into quark pairs, leading to a four quark final state. This is one of the signatures to which this analysis is sensitive.

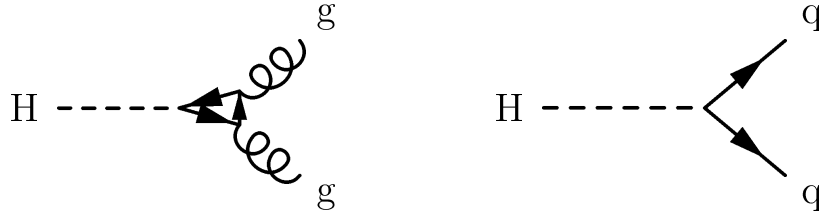


Figure 3.2: The two decay modes of a Higgs boson considered in this analysis. *left*: the Higgs boson decaying into a gluon pair with a quark loop as intermediate state. *right*: the Higgs boson decaying into a quark-antiquark pair.

Higgs-strahlung might lose its importance in 2HDM because there exists a complementary process, the *associated hA -production*:

$$e^+e^- \rightarrow Z^* \rightarrow hA \quad (3.1)$$

The relative strength of the two processes depends on the chosen model parameters α and β . While the coupling is proportional to $\cos(\beta - \alpha)$ for Higgs-strahlung, it depends on $\sin(\beta - \alpha)$ in case of the associated production of h and A . Thus in 2HDM Higgs-strahlung remains the dominant production channel only if $\cos(\beta - \alpha)$ is large.

This search is sensitive to two different decay modes of the Higgs boson, the production of a quark-antiquark pair or of a pair of gluons via a virtual quark loop (fig. 3.2):

$$\begin{aligned} h &\rightarrow q\bar{q} \\ h &\rightarrow gg \end{aligned} \quad (3.2)$$

The Z boson is assumed to decay into hadrons (fully hadronic channel). Therefore this process leads to four jet events ¹.

¹In the following, the term "jet" is used to refer to a final state with a primary quark or gluon. See also the next sections.

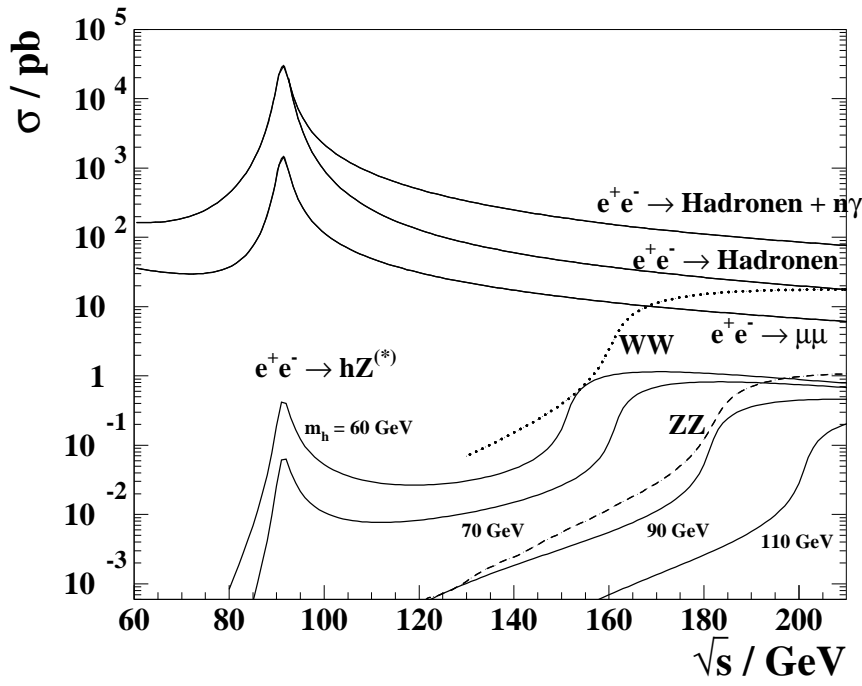


Figure 3.3: The cross sections for Higgs-strahlung in comparison to Standard Model processes. Higgs masses between 60 GeV and 130 GeV are assumed. The cross sections are given as functions of the center of mass energy \sqrt{s} in the energy range accessible with LEP.

3.1 Simulating Particle Interactions

When electrons and positrons collide at typical LEP2 energies, a large number of processes occurs that must be taken into account in order to derive a theoretical probability density function that can be compared with experiment. Due to the complex interplay of the possible interactions this must be done numerically. Hence *Monte Carlo simulations* are used, that simulate the processes up to a certain precision.

A Monte Carlo procedure [26] starts by generating random numbers in the range $0 < x < 1$ which are further used to define a probability density function $f(x)$ which takes values in the desired range. The values of x can be considered as simulated events. Integration of $f(x)$ then yields the desired distributions after a number of interactions.

The experimental result is simulated in two stages: the *event generator* that yields the spectrum of final states for a given interaction, and the *detector simulation* that models the detector response. This refers primarily to the interactions of the primary and secondary particles as they pass through the detector system. The detector simulation is done by the GOPAL program [27], which is based on the standard particle interaction simulation package GEANT 3 [28].

Different event generators have been used for this analysis. The Higgs interactions were simulated using the HZHA generator [29], the background processes with GRC4F [30] (four fermion processes) and KK2F [31] (two fermion interactions).

The generators above simulate only the two or four quark/gluon final state. The final state containing hadronic jets depends on the details of the QCD evolution of the colored system, for which no theoretical description exists, unlike in the case of the electroweak interactions.

3.1.1 Parton Showers and Hadronisation Schemes

When quarks are produced in an interaction, they cause a large number of secondary processes, due to QCD interactions. As a result of confinement single quarks cannot exist, therefore a quark produces a large number of hadrons. The visible outcome in the detector are the "jets", bunches of tracks that trace back to a common origin and spread out with a certain opening angle.

QCD processes cannot be handled by perturbation theory on all energy scales, because the strong coupling constant increases with decreasing energy. But perturbation theory can be used at high energies. If the energy drops below ~ 1 GeV, then the behaviour of the particles can only be approximated by models. The modelling procedure will be sketched here for a frequently used algorithm as given by PYTHIA/JETSET [32].

Two different procedures are used to describe the development from primary quarks or gluons to the final hadrons in the jets:

- *Parton Showers*,
descending branches as $q \rightarrow gg$ and $q \rightarrow q\bar{q}$ for processes at higher momenta
- *Hadronisation (or Fragmentation)*,
the combination of quarks into observable hadrons at lower momenta.

The structure of parton showers is given in terms of branchings such as $q \rightarrow qg$ or $g \rightarrow q\bar{q}$. Quarks and antiquarks are treated alike. The processes are each characterized by a splitting kernel $P_{a \rightarrow bc}(z)$ that is derived from the theoretically predicted shower evolution [33]. A more detailed discussion about its application can be found in [32]. The splitting kernel yields the total branching rate by

$$\int_{z_-}^{z_+} P_{a \rightarrow bc}(z) dz \quad (3.3)$$

The z value describes the energy sharing of the daughter partons b, c . These daughter partons again can branch. The integration is carried out over all allowed energy sharings during the shower.

The partons are further characterized by a "virtuality scale" Q^2 , given in GeV^2 . This scale approximately provides a time ordering for the shower and it decreases with time. Q in addition defines the energy range of the shower: Q_{max} gives its upper value, when the shower must be matched with the initial hard interaction. The choice of Q_{max} has a big influence on the jet separation, but the relation between Q_{max} and the kinematics of the hard scattering is uncertain. Q_{min} defines the cut off value for the shower, which is chosen to be around 1 GeV.

Q^2 is related to the mass squared of the parton, but not in a unique way. During the shower evolution, the Q value of a parton decreases until a branching occurs. The Q^2 value yields the mass of a branching parton, which together with the value of z describes the branching process. The daughter partons evolve in an analogous way with the virtuality parameter given by the kinematics, until the cut off parameter Q_{min} is reached.

This procedure breaks down for longer distances, i. e. in later states of the shower process. Due to confinement, colored partons are transformed into colorless hadrons. This procedure is called hadronisation (or fragmentation). Theoretically it is not well understood, therefore a number of models exist for the phenomenological description.

The scheme presented here is the "Lund model" (string fragmentation): Assume a color singlet $q\bar{q}$ 2-jet event and apply a linear confinement model, i. e. a color flux tube being stretched between the quark and the antiquark as they move apart from their production vertex. If the tube is assumed

to be uniform along its length, then the potential rises linearly with the distance between the quarks. As the potential energy between the quarks rises, it can lead to $q\bar{q}$ pair production, when the energy exceeds the mass equivalent of the quarks. Then the string breaks, leading to a new string with quarks on each side. Depending on the energy, new breaks can occur, until only stable on-mass-shell hadrons remain.

The quark pair production is described within the Lund scheme as a quantum mechanical tunneling process. Due to the different masses, the production of light flavoured quarks is therefore expected to dominate. Hence, heavy quarks are produced only in hard processes.

Since the subsequent string breaks are not conditioned by each other, technically an arbitrary sequence can be chosen. So they can be assumed to proceed from one string end to the other. Since it is arbitrary whether to start at the quark or at the antiquark end, this constrains the possible form of the fragmentation functions. Finally two free parameters remain which must be determined empirically.

3.2 Standard Model Interactions at 200 GeV

When electrons and positrons collide with center of mass energies of around 200 GeV, a large number of Standard Model processes can occur. An overview can be obtained from fig. 3.6. Those events are considered as "background processes" if one is looking for new particle interactions such as the production of a Higgs boson. In order to separate the Standard Model processes from those which are searched for, one must first find a way how to distinguish them. Thus, a profound knowledge of the phenomenology of both the background and the signal is required.

For the present analysis it is appropriate to separate the background into two classes, according to whether the final state has two or four fermions.

3.2.1 The Two Fermion Background

As can be seen in fig. 3.6, the production of $q\bar{q}$ -pairs provides the major contribution to the background even though its cross section drops with increasing energy. This is due to two different processes [34]. First, the distance to the peak of the Z resonance at 91 GeV increases, hence fermion pair production decreases rapidly, while photon exchange gains importance.

Second, corrections due to Initial State Radiation (ISR) must be taken into account. ISR occurs when particles in the initial state radiate one or more photons. Since hard photons are emitted preferably at energies which are well beyond the Z resonance, the effective center of mass energy for the two fermion process is lowered. As the Z width provides a natural cut off for hard photons, this decrease in the center of mass energy is oriented towards the Z resonance ("Z return"). Including ISR enhances the muon

cross section as obtained by first order in perturbation theory roughly by a factor of two. If it is taken into account, two fermion production remains the strongest contribution from Standard Model processes also at energies above 200 GeV.

A pure two fermion process leads to a final state with two rather than with four quarks. One or both fermions can radiate hard gluons, thus increasing the number of jets. Some of the Feynman graphs are shown in fig. 3.4.

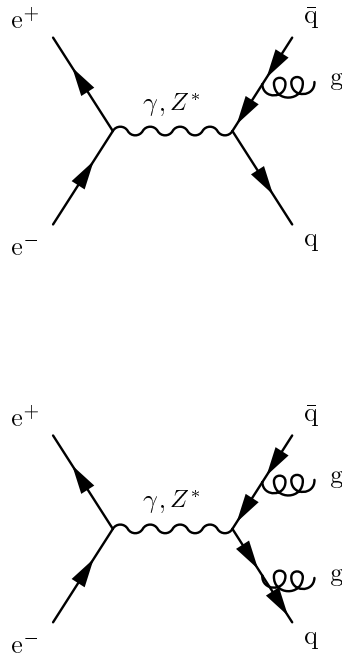


Figure 3.4: $q\bar{q}$ production with gluon radiation. The Feynman graphs show examples of two fermion events with final state radiation. Processes of this type lead to the quark antiquark background by faking four fermion topologies in the detector.

3.2.2 The Four Fermion Background

The second class of background in a Higgs search examining the hadronic channel are four fermion processes. These occur mainly when W or Z pairs are produced and decay into hadrons.

Since those processes are quite similar to the Higgs-strahlung, they are harder to separate from a possible signal than the two fermion background.

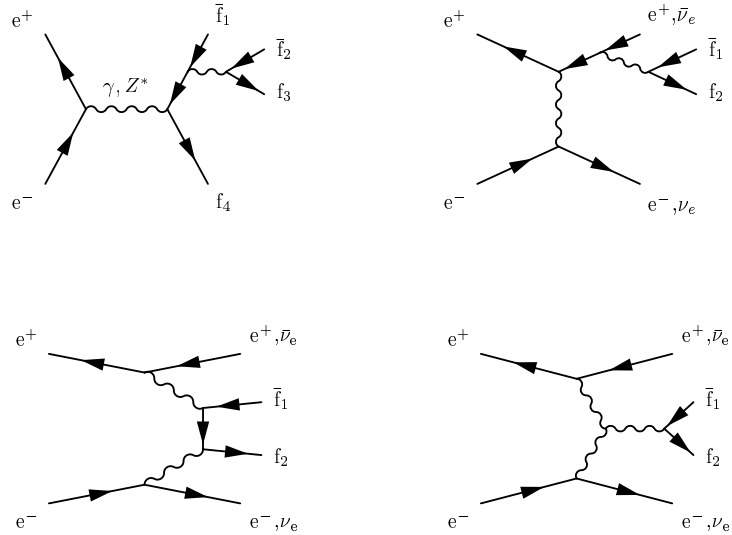


Figure 3.5: Feynman diagrams of some of the possible four fermion final states that contribute to the four fermion background.

Apart from the W/Z pair production, a number of more complicated interactions can lead to hadronic four fermion topologies. Their Feynman graphs are given in fig. 3.5.

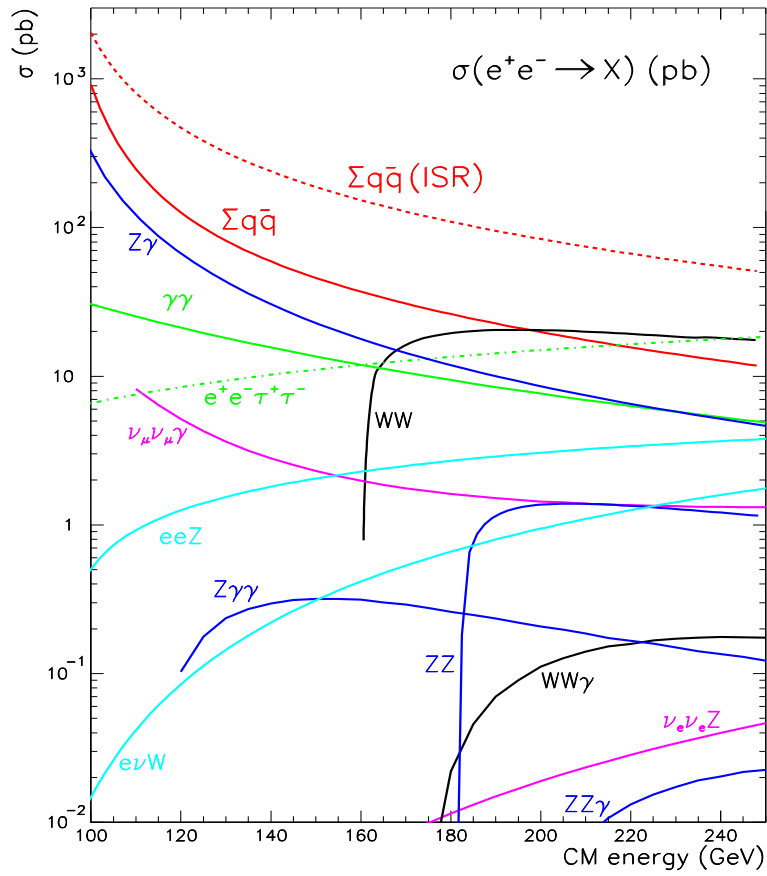


Figure 3.6: Contributions from Standard Model processes at LEP2 energies. At around 200 GeV and neglecting initial state radiation, $q\bar{q}$ production becomes less important than the production of W pairs. Both processes lead to final state topologies with four jets and are therefore important for the analysis under study. A third process to be considered is the production of Z pairs with a cross section of about a tenth of the WW cross section.

3.3 Properties of Neutral Higgs Decays

This analysis considers kinematic variables exclusively and it *does not* make use of a feature on which the Standard Model Higgs searches heavily rely: the explicit identification of bottom quarks. In the jargon of the trade this is referred to as "b tagging". Bottom quarks have a lifetime that is long enough to allow the detection of "secondary vertices". These occur when a particle flies far enough between its production and decay so that the primary vertex (the production point) and the place of its decay (secondary vertex) can be distinguished.

At LEP energies, the production of top quark pairs is kinematically not possible. In the Standard Model the Higgs boson preferably couples to particles with the highest mass. The best candidate at LEP is therefore the b quark. Especially events with four b quarks in the final state (two from the H and two from the Z) should occur more often when a Higgs boson is produced, because the background processes (e.g. W/Z pair production) do not prefer b quarks to the same degree.

Within 2HDM, the use of b quarks can be misleading, even though the Higgs boson still preferably decays into the heaviest particles. However, since the coupling strengths depend on the model parameters it is well possible that the decay to down type fermions (like the b quark) is very suppressed. Therefore a *flavour independent analysis* is suitable rather than the tagging of b quarks. In principle such an analysis is sensitive to any electrically neutral massive scalar boson.

In order to improve the use of the kinematic variables under study, a *test mass dependent* analysis is done. Explicit hypotheses of the Higgs mass are made and the data is analysed separately for each test mass. This does not only allow a more precise adaption of the variables to the actual kinematic situation, but also leads to new variables that explicitly depend on the mass of the Higgs boson. For a search within 2HDM this becomes even more important because Higgs masses of about the gauge boson masses are already excluded for a wide parameter range [35].

Not only do the different masses yield a discrimination power between the Higgs signal and background events, but also the topology of the final state. This applies namely to the four fermion background, that mimics Higgs events to a high degree. The light neutral Higgs boson is a scalar, whereas the gauge bosons as main background processes are vector particles. This leads to a higher isotropy in the final state topologies of the Higgs boson.

Chapter 4

The Experimental Requirements

The present analysis was performed with data of the OPAL detector ("Omni Purpose Apparatus for LEP"). This complex ensemble of a number of detector types was one of the four main experiments of the "Large Electron Positron Collider" (LEP), a 27 kilometer long storage ring situated at the European Organization for Nuclear Research (CERN) outside Geneva. It was under operation from 1989 until past November. The main task for LEP was to test the Standard Model by high precision measurements and to search for phenomena beyond the Standard Model. For this, electrons and positrons were collided at four interaction points with center of mass energies between 91 and 209 GeV.

Bunches of electrons and positrons were accelerated by a sequence of accelerators (Fig. 4.1), until they were each injected with an energy of 22 GeV into the LEP ring and further accelerated until they reached the final energy. Then the two particle beams were collimated by a set of quadrupole magnets, focusing the bunches at the interaction points. There beam crossings took place with a frequency of around 45 kHz.

Two different strategies were pursued during the 12 year long operation of LEP: in the first run, from 1989 until 1995, collisions were performed with a center of mass energy of 91 GeV, i. e. at the rest mass of the Z boson. After an upgrade of both the accelerator and the detectors, further studies at higher center of mass energies started with a second run late in 1995, until a maximum of around 209 GeV was reached in 2000. One emphasis of the second run was to measure the properties of W bosons, being produced in pairs, thus requiring a center of mass energy of about 161 GeV. Additionally, searches for new particles were performed. They did not lead to a discovery, but decreased the possible parameter space for many theories.

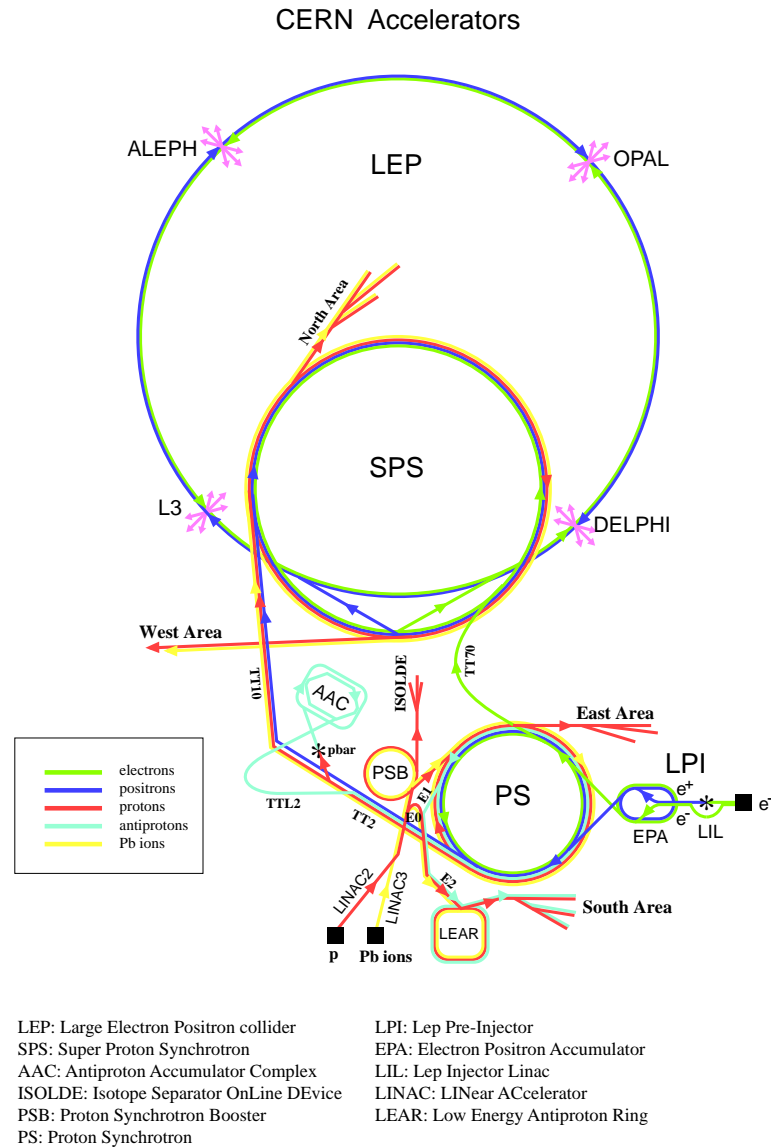


Figure 4.1: The LEP storage ring and the chain of accelerators used before the injection into the main ring. The blue line shows the path of the positrons and the green line refers to the electrons. The acceleration starts in the linear accelerators of the LPI system. Then the particles are injected into the PS and further into the SPS. When they are injected into the main LEP ring, they have reached an energy of 22 GeV per beam. The other parts of the system are used for different experiments at CERN.

4.1 The OPAL Detector

The OPAL detector [36] is a combination of seven different detector types, onion-like arranged in layers around the interaction point. As particles pass through the different subdetectors, they leave different signatures. Combining these signatures allows the reconstruction of the physical properties of the event, such as the momentum, energy and identity of the produced particles. OPAL's overall shape is a cylinder ("barrel") of about 12 meters length and about 12 meters in diameter, closed by "end cap" detector systems on each side. This assures that 98 % of the space around the interaction point is covered by detectors [36], to minimize the risk that particles escape undetected. A small region must remain open due to the beam pipe.

Special devices were placed close to the beam pipe in the endcap regions to measure the luminosity ¹. For this purpose small angle Bhabha scattering served as the reference process.

Each point within the detector is defined by its (cylindrical) coordinates. The z axis points into the e^- direction, the polar angle θ gives the angle with respect from the beam axis, and the azimuthal angle ϕ about the z axis. The direction with $\phi = 0$ and $\theta = \pi/2$ points towards the center of the LEP ring. Fig. 4.3 shows a candidate for a Higgs event, which was recorded at a center of mass energy of around 205 GeV. The left picture gives the axial view, as obtained by a cut perpendicular to the z axis through the vertex.

The layers of different detector types appear as concentric circles, oriented around the beam pipe (inner circle). One difference between the inner and the outer part is evident: towards the center, single *tracks* are recorded, providing a detailed spatial resolution. In the periphery, larger parts of the detector respond when a particle passes through. Only a coarse spatial information can be obtained, but the detector layers provide a signal proportional to the total energy of the particles. Not more than a few signals appear in the outer region. Apparently most particles have been stopped before reaching the outer layer. These three different signal types are provided by a number of detector types that will be described in the following.

4.1.1 The Inner Tracking System

A good determination of an event's kinematic properties is essential for this analysis. This is mainly done with the Inner Tracking System (c. f. fig. 4.2, 4.3). It consists of four components:

- the silicon microvertex detector
- the vertex chambers

¹The luminosity is the ratio of the number of events per unit time N and the cross section σ : $\mathcal{L} = \frac{N}{\sigma}$

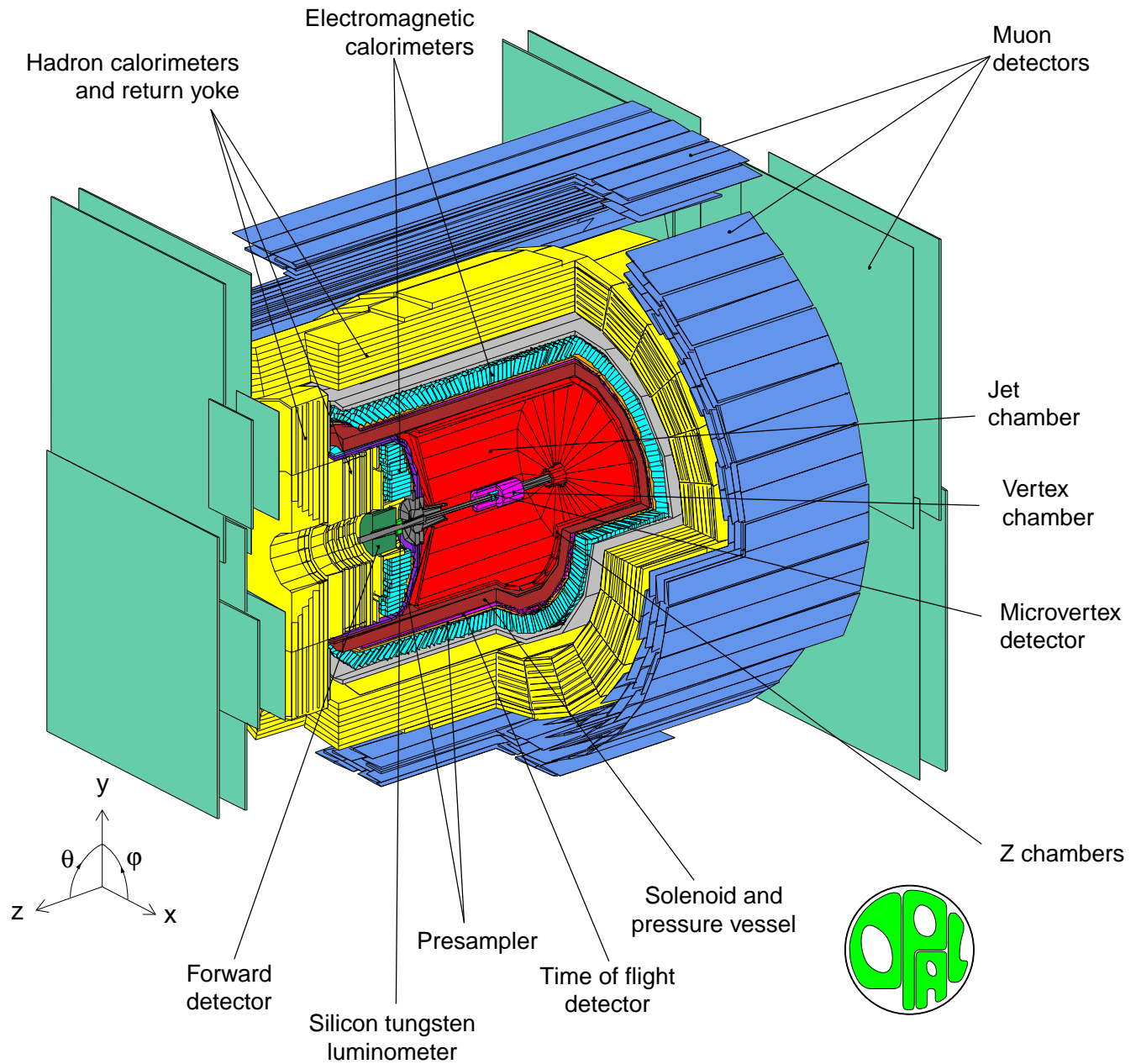


Figure 4.2: The Omni Purpose Apparatus for LEP (OPAL) and its subsystems, built around the beam pipe of the LEP accelerator. For this analysis especially the tracking system and the two calorimeters are used.

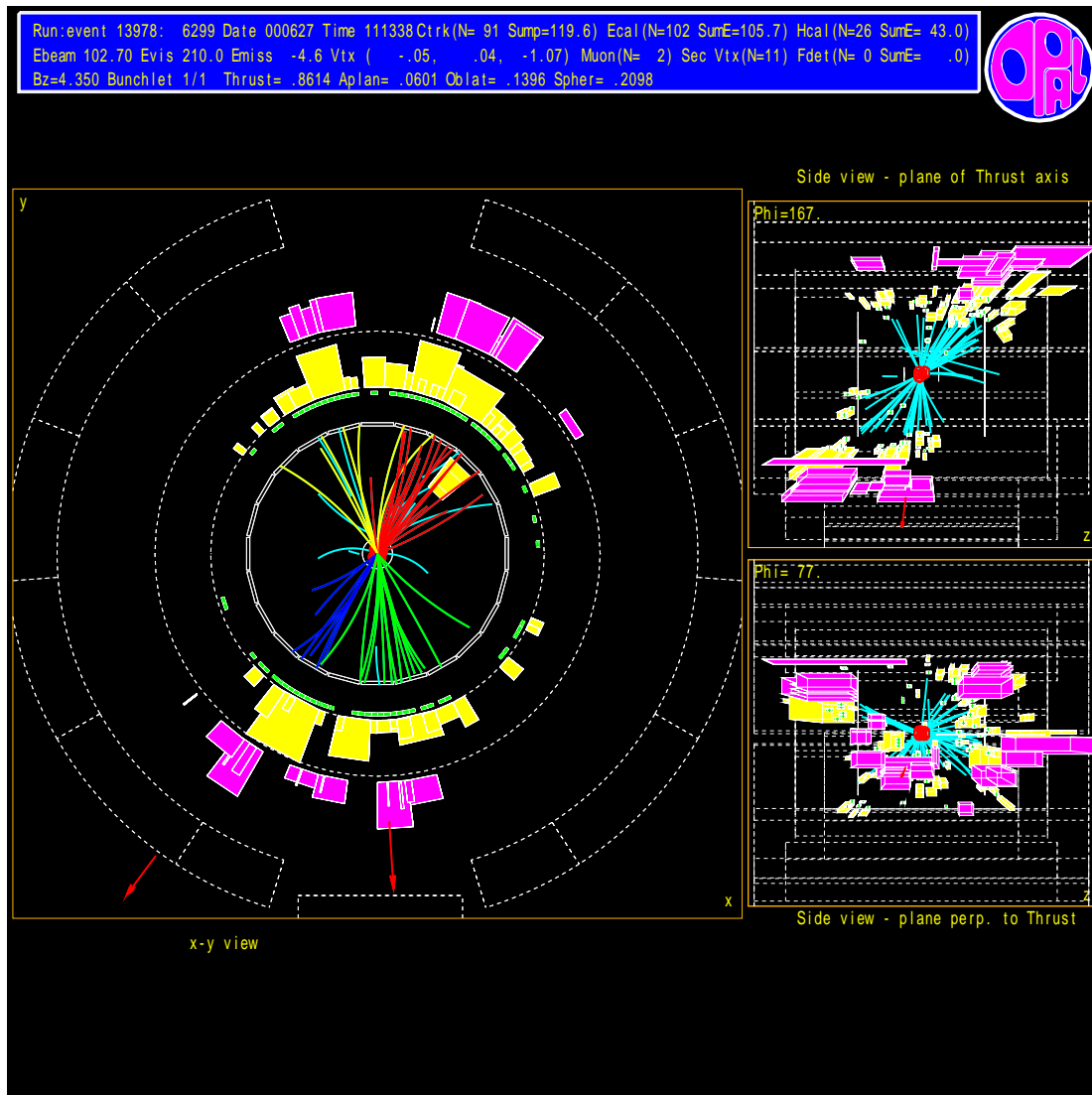


Figure 4.3: A candidate that was selected with this analysis at a center of mass energy of about 205 GeV. The reconstructed Higgs mass is 113.35 GeV. The tracks have been assigned to four jets, as indicated by the different colors. The energy deposited in the different calorimeters and the muon chambers can be seen in the outer layers. A more detailed description is given in the text. The views presented here are (a) the axial view through the vertex (b) a side view in the jet plane and (c) a side view perpendicular to it.

- the jet chambers
- the z chamber

The *silicon microvertex detector* [36] consists of two layers of silicon strips, laid concentrically around the beam pipe. It covers a polar angle of $|\cos\theta| < 0.89$. Its main purpose is to measure secondary vertices, as needed when an analysis uses explicitly the identification of b quarks (e. g. searches for the Standard Model Higgs boson). Since the present analysis is independent of the quark flavour, the main use of this detector is its high spatial resolution.

The *vertex, jet and z chambers* are all based on the same detector principle. They are drift chambers, made of alternate signal and field wires. As a particle passes through the detector, it ionizes the gas atoms and due to the electric field of the field wires, the charge clouds drift to the signal wires. With a constant drift velocity a spatial resolution can be obtained that is far beyond the spacing of the signal wires. The tracking system is placed inside a homogenous magnetic field of 0.435 T, imposing a circular motion on the charged particles and allowing the measurement of their momenta.

As the three chamber types are optimized for different purposes, they differ in their structure. The vertex chamber must provide an extremely good spatial resolution, because the first points of a track are crucial to determine decay vertices in the beam pipe. Therefore, the spacing of the wires is twice smaller (about 5 mm) than in the jet chambers (10 mm). The jet chambers, on the contrary, must provide a large volume.

Vertex chambers and jet chambers must both provide information about all three dimensions. Therefore, cells with the wires along the beam direction ("axial cells") and cells with a wire plane inclined by 4° ("stereo cells") are combined. The combination of both allows a coarse information about the z coordinate.

The coordinates of every point are measured from the wire position, from the drift time and from the determination of the "charge division": The integrated charges for each hit are measured at both ends of the signal wire. The z coordinate is then determined by the ratio of the charges. Furthermore, the sum of the two charges is used to measure the energy loss in the chamber (dE/dx).

The z resolution is enhanced by the *Z chambers*, that are only in the barrel region. Wires are strained along the azimuthal direction, thus enhancing the spatial resolution along the z axis. The spatial resolution is further improved by placing the whole tracking system into a pressure vessel with a pressure of 4 bar.

The overall performance of the tracking system is such that 98 % of the solid angle is covered, yielding a spatial resolution of 60 μm for the z coordinate of the first point of a track. The distance perpendicular to the z axis is given with a precision of 20 μm . A minimum of eight hits per track are required, the maximal hit number being 159. The resolution of

the energy loss dE/dx , important for the particle identification, is given in a range between 3 and 4 % [36].

4.1.2 The Calorimeters

The energy of a particle can only be measured if it is completely deposited inside the detector. This is the purpose of the two calorimeters, the electromagnetic calorimeter and the hadronic calorimeter.

The *electromagnetic calorimeter* is situated between the coil and the return yoke of the solenoid. It consists of lead glass blocks, provoking electromagnetic showers when electromagnetically interacting particles pass through. Therefore it mainly detects electrons, positrons and photons and measures their position and energy.

The energy resolution of the electromagnetic calorimeter is about $\frac{\sigma_E}{E} \sim 0.2\% + \frac{6.3\%}{\sqrt{E}}$ [36]. The spatial resolution is around 1 cm. 98 % of the solid angle is covered. About four radiation lengths of material are placed between the vertex and the calorimeter, therefore many showers are already initiated in the inner detector parts, especially within the coil of the solenoid magnet. This is compensated by placing a *presampler* at the calorimeter's inner side.

Also hadrons lose a part of their energy in the electromagnetic calorimeter before they penetrate the hadronic calorimeter. Electrons, positrons and photons on the contrary are stopped in the electromagnetic calorimeter. This becomes evident by comparing the number of interaction lengths provided by the 37 cm long lead glass blocks: they represent *24.6 radiation lengths* for electrons, but *less than 2.2 interaction lengths* for hadrons [36].

The *hadronic calorimeter* is the main device to record the energy of the jets. Only hadrons and muons can pass through the electromagnetic calorimeter. The hadrons are to the biggest part stopped inside the hadronic calorimeter. This detector is placed within the magnet return yoke and consists alternately of iron slabs and streamer tube detectors. As hadrons pass through the iron, they cause nuclear interactions, thus leading to hadronic showers of secondary particles. These are recorded in the streamer tubes. The total hadron energy is obtained by adding the energy deposited in the electromagnetic and in the hadronic calorimeters. An energy resolution of $\frac{\sigma_E}{E} = \frac{130}{\sqrt{E}}$ % [36] can thus be obtained for 10 GeV incident energy [36].

4.1.3 The Muon Chambers

In principle, no hadron should pass through the hadronic calorimeter. Therefore the *muon chambers*, being large area drift chambers operated with an ethane-argon mixture, should not respond at all. In spite of this, there are signals in the outermost regions of fig. 4.3, indicating that indeed there have been interactions. This can happen by three mechanisms:

- *sneakthrough*: hadrons do not interact strongly in the hadronic calorimeter.
- *punchthrough*: secondary shower particles emerge from the hadronic calorimeter and fake a muon.
- *decay in flight* of pions and kaons resulting in muons.

The last case is realized mostly for low momentum particles. Since the OPAL detector was designed for interactions at around 91 GeV, the first two scenarios are more likely to have caused the signals. In particular the second one occurs preferably at high momenta.

The muon chambers cover 98 % of the solid angle. Discriminating between muons and hadron interactions requires a track interpolation from the inner detector parts to the muon chambers. A good spatial resolution is therefore needed, being 2 mm for measurements along the z axis and 1.5 mm perpendicular to it [36].

4.2 The OPAL Trigger

Each 22.2 μs bunches crossed inside LEP, leading to a crossing rate of 45 kHz. To select crossings with a possible e^+e^- interaction, a flexible and programmable trigger system is needed. Its purpose is to reduce the event rate down to 1 to 5 Hz, so that the data acquisition system can handle the amount of data. Furthermore the background from cosmic muons is to be reduced, as well as interactions of the beam particles with the wall of the beam pipe or with the gas within. In order to enhance the detection efficiency and to better monitor it, most trigger signals are taken redundantly with different subdetectors. For multihadron events as used in this analysis the OPAL trigger efficiency exceeds 99.9 %.

In the central trigger logic, the trigger signals from the subdetectors are logically combined. Those signals are divided into two classes: first, the whole solid angle is divided into 144 overlapping regions in the θ and the ϕ direction. The signals are ordered within this scheme and summed for each region. Second, the trigger signals from the various subdetectors are considered independently of their orientation and place.

4.3 Correction for Double Counting

Depending on their properties, particles induce signals in multiple parts of the detector. The information that is carried by these signals has to be combined in order to get the best estimate of the particle energy and momentum. For example charged hadrons are measured in the tracking system and they deposit energy in both the electromagnetic and the hadronic

calorimeter. A simple sum of the energies would often lead to an energy double counting.

A proper matching of the detector responses for a single particle and the correct energy measurement are crucial for this analysis, as it relies exclusively on the event kinematics. Therefore an algorithm was applied to account for the above effects [37, 38]. First it extrapolates the tracks from the inner detector to the calorimetry surface. Size and position of the clusters are then compared with the extrapolated tracks.

In a jet environment as considered in this analysis, the tracks in the clusters do overlap. The expected energy response and the spreads of all showers are therefore taken into account for each possible combination of tracks and clusters.

The energy is reduced using the best matching clusters and tracks. This is done in an iterative procedure. The assignment of clusters to tracks is more precise if the track momentum is low. Therefore the algorithm starts with those particles that left the lowest momentum tracks in the central tracking region. First the energy is subtracted from the hadronic calorimeter. If this is not enough, then the energy in the electromagnetic calorimeter is also reduced.

Special care must be taken for hadrons, because the energy responses of the hadronic and the electromagnetic calorimeter are significantly different. The energy scale for the clusters is adjusted using empirical correction factors obtained from a Monte Carlo simulation.

The performance of the correction is further enhanced by identifying the primary particles. This information is used to account for the expected energy resolution and the shower spread of the assumed particle.

With this procedure an overall energy resolution of 8.6 GeV can be obtained for events with an energy of 90 GeV, which equivalent the Z mass.

4.4 Data Samples of this Analysis

This analysis uses the approximately 210 pb^{-1} of OPAL data recorded in the year 2000 at center of mass energies between 202 and 209 GeV (fig. 4.4). The average center of mass energy was 206.1 GeV. With a Z mass of 91 GeV, Higgs bosons could have been produced if their mass is at least 91 GeV below the center of mass energy. This mass indicates the upper limit of the kinematically allowed range and is therefore called the "kinematic limit".

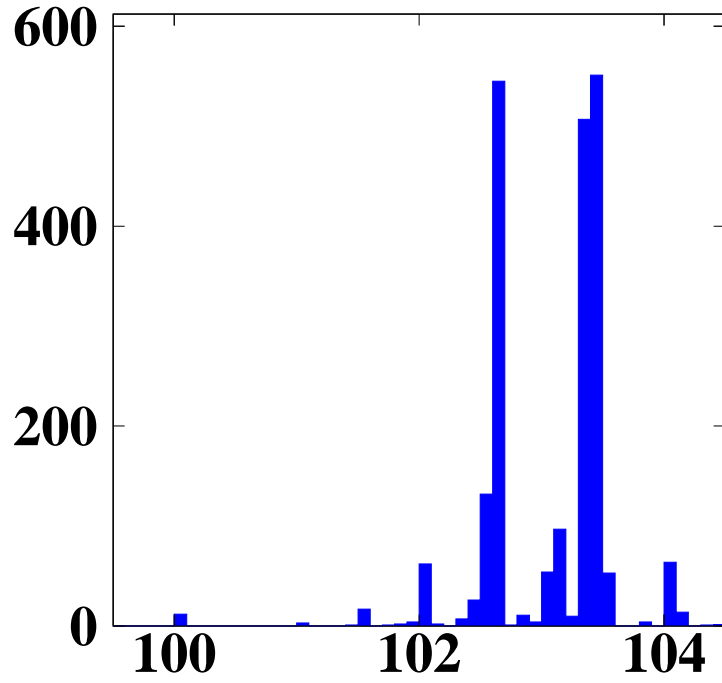


Figure 4.4: Energy distribution of the year 2000 data. Here the energy per beam is given, being half the center of mass energy. The luminosity is scaled in arbitrary units. The average energy in the center of mass system is 206.1 GeV.

Chapter 5

The Analysis Method

Different interactions will lead to different properties of the final states. These properties can be transformed into variables whose values allow in some cases the unique distinction of a signal from the background. If this is the case, then the background events can easily be discarded by defining a range of "signal like" values. Only events within this range are kept for a further analysis, the others will be "cut". A sequence of cuts can be applied until in the optimal case the signal only is kept.

Such a clear distinction is not possible in the present analysis, because the distributions for the three event classes (Higgs-strahlung process, four fermion background, $q\bar{q}$ background) overlap for all variables to a high degree. An efficient distinction, based only on cuts, is not possible. Hence, this analysis is a composite of two different techniques:

- **a cut-based preselection** consisting of six variables, to reject events that differ considerably from those under study, followed by
- **a likelihood selection** based on a *likelihood ratio method* with seven variables, when a clear and unique distinction between signal and background is not possible.

5.1 Elements of a Higgs Search beyond 200 GeV

5.1.1 Identifying Jets

Recognizing jets is not an easy task, even more because they often overlap. Several algorithms have been developed. The one used here is optimized to the mass reconstruction of W and Higgs bosons as well as to the selection performance for the Higgs four jet channel [39].

First, the "core" of a jet is defined, using a traditional jetfinder. These jets are considered as "reference jets" for the further procedure. Then the particles anew are associated to the cores, they are "reassigned", as described below.

The building of the core is done using the DURHAM algorithm [40, 41]. A scaled transverse momentum y_{kl} is defined by

$$y_{kl} = 2(1 - \cos \theta_{kl}) \min(E_k^2, E_l^2) / s \quad (5.1)$$

Where $E_{k,l}$ are the center of mass energies of the final state particles k and l . s is the square of the total center of mass energy of the event, and θ the angle between the particles.

A value of y_{kl} is calculated for each pair of particles (k, l) . Those two particles that yield the smallest value are combined and replaced by a pseudoparticle with the momentum $\vec{p}_k = \frac{E_k}{|\vec{p}_i + \vec{p}_j|} \cdot (\vec{p}_i + \vec{p}_j)$ and the energy $E_m = E_k + E_l$. This procedure is repeated until the y values for all particles or pseudoparticles exceed a given threshold value y_{cut} . The remaining objects are considered as "cores" and used as the reference jets. This scheme, not being Lorentz invariant, can only be used in the laboratory frame. The total momentum sum of an event is not conserved. It is widely used though, because by and large it is independent of the chosen hadronisation model [40].

Once the four reference jets are defined, the particles are reassigned using the JADE E0 algorithm [42]. Particles are added to a jet if the assignment with the chosen jet minimizes the expression with respect to the other jets:

$$E_i^{jet} \cdot E_{particle}^j \cdot (1 - \cos \theta_{ij}), \quad (5.2)$$

E_i^{jet} being the energy of the i -th jet ($i = 1, 4$) and $E_{particle}^j$ the energy of the particle.

5.1.2 Kinematic Fits

Kinematic fits play a key role in this analysis. They help to separate signal and background events and to properly assign tracks to the jets. Furthermore, they are needed for a more precise reconstruction of properties of final state particles, such as the jet energy or angular distribution.

Each of the four jets in an event provides three parameters that can be fitted. It proved to be a good choice [43] to use $\vec{x} = (\log p, \theta, \phi)$. p being the jet momentum, and θ and ϕ its coordinates as given in section 4.1.

The fit should vary the parameters to a minimum and fulfill the constraints (for example total energy and momentum conservation). This is carried out by the χ^2 method, the χ^2 being composited of two terms:

$$\chi_T^2 = (\vec{x}_{meas} - \vec{x}_{fit})^T V^{-1} (\vec{x}_{meas} - \vec{x}_{fit}) \quad (5.3)$$

and

$$\chi_K^2 = 2|\vec{\lambda} \cdot \vec{F}| \quad (5.4)$$

χ_T^2 is the discrepancy between the measured and the fitted parameter values, accounting for the errors as given by the error matrix V . The two vectors contain the measured and the fitted parameters.

χ_K^2 contains information about how well the constraints are fulfilled. $\vec{\lambda}$ are Lagrange multipliers, \vec{F} gives the constraints.

The fitted parameter value \vec{x}_{fit} are found by minimizing χ^2 for each component of $\vec{\lambda}$ and \vec{x} . This yields a set of equations that in general can only be solved by iteration. The procedure stops either when the fit has converged or when the number of iterations exceeds a given maximum.

Convergence is reached when a number of requirements are fulfilled:

- little change of χ^2 from one iteration to the next (here < 0.001)
- little change of χ_T^2 (here < 0.0001)
- χ_K^2/χ_T^2 should not exceed 0.01

If the fit converged, then a probability can be stated that a random variable with a N dimensional χ^2 distribution acquires a value X larger or equal the minimal value of χ^2 :

$$P(X|N) = \frac{1}{\sqrt{2^N}\Gamma(\frac{1}{2}N)} \int_X^\infty e^{-\frac{1}{2}t} t^{\frac{1}{2}N-1} dt \quad (5.5)$$

The χ^2 will serve in the analysis to quantify the probability that the constraints of a hypothesis are fulfilled.

Kinematic fits have been applied in four different ways in this analysis:

- **as a four constraint fit:**
forcing the components of the four momentum to be compatible with the measured centre of mass energy,
- **as a five constraint fit:**
as the one before, with the additional restriction that the mass of one of the jet pairs be equal to the mass of the Z boson,
- **as a six constraint fit:**
in addition to the constraint on the four momenta, both jet pairs must be equal to the mass of the W boson for this jet combination,
- **as a 5.5 constraint fit:**
as the four constraint fit, but forcing one jet pair to the hypothetical mass of the Higgs boson, the other one to a mass within the width of the Z boson ("soft" mass fit).

5.1.3 Matrix Elements

Matrix Elements yield the theoretical description for the transition from one state of a quantum system to another. For many particle interactions, the matrix elements are given explicitly, at least in first order of perturbation theory. They include predictions about kinematic features of an event, and are therefore very useful for this analysis. Three different matrix elements are used:

The matrix element for all four fermion events as calculated in the EXCALIBUR [44] event generator

Their calculation accounts for all possible four fermion final states as emerging in e^+e^- collisions. The procedure includes QED corrections due to initial state radiation as well as QCD diagrams due to the four fermion final state.

This matrix element mainly helps to reduce the background due to quark antiquark pair production, while the distributions for Z and W pairs widely overlap with the signal values. Due to the large energy loss into Initial State Radiation, most of all for the quark pairs, it is not useful to impose any further kinematic fit [45]. The center of mass energies of the events vary too strongly.

The matrix element for WW using a fit with four constraints

This matrix element is calculated in analogy to the previous one, using only the W pair diagrams. The four momenta were corrected with a four constraint fit.

The matrix element for Higgs-strahlung using a soft kinematic fit

As further described in [45] and [46], the Higgs-strahlung matrix element discriminates between the signal and the background mainly by their angular distribution. The Higgs boson is predicted to be a scalar, therefore it must decay isotropically, unlike all background contributions. They lead to rather unisotropic final states, the gauge bosons due to their vector nature, and the quark pairs because of their pencil like event shape.

The matrix element for hZ events only depends on the invariant mass and the decay angle of the Z boson. The soft mass constraint as described in section 5.1.2 accounts for the width of the Z. Therefore the dependence on the reconstructed Z mass can be reduced by using the 5.5 constraint fit.

5.2 The Preselection

5.2.1 Variables in the Preselection

A cut-based preselection method was chosen, following a standard procedure in the four jet analyses of OPAL Higgs searches [47]. It is a combination of six steps.

Cut 1: Hadronic Final State

Being a set of three requirements with a wide range of application within OPAL at LEP2, this is a rough first estimate about the nature of a process. The goal is to distinguish fully or semi-hadronic events from processes such as two photon events: $e^+e^- \rightarrow \gamma\gamma$. Namely, the criteria are

- high multiplicity:
At least seven electromagnetic clusters and five tracks must be recorded. This serves as a lepton rejection.
- energy deposit in the electromagnetic calorimeter:
More than 14 % of the center of mass energy must be deposited in the electromagnetic calorimeter. This especially cuts away the background from two photon events.
- energy balance along the beam axis:
This helps to rule out hits inside the beam pipe, and contributes to a further rejection of two photon events. It is required that

$$R_{bal} = \frac{|\sum(E_{clus} * \Theta)|}{\sum E_{clus}} < 0.75, \quad (5.6)$$

Θ being the polar angle of the cluster.

Cut 2: Center of Mass Energy in the Final State

The energy in the final state must exceed 79.4% of the center of mass energy in the collision. Thus events with gamma-emission from the initial state are further excluded.

Cut 3: Jet Separation

The y_{cut} parameter (see 5.1.1) as defined by the DURHAM algorithm (c.f. [40, 41]) must exceed 0.003.

Cut 4: Event Shape C Parameter

The C shape parameter gives a measure for the global event shape of QCD events with two or more jets [48, 49, 50]. Mathematically, it is a tensor based on the momenta of all final state particles:

$$C = 3(\lambda_1\lambda_2 + \lambda_2\lambda_3 + \lambda_3\lambda_1), \quad (5.7)$$

λ being the eigenvalues of the linearized momentum tensor

$$\Theta^{\alpha\beta} = \frac{\sum_i p_i^\alpha p_i^\beta / |p_i|}{\sum_j |p_j|},$$

summing over all particles in the final state.

The C shape parameter takes values in the range $0 \leq C \leq 1$, with $C = 0$ for a perfectly collinear two-jet like final state. If the jet momenta are distributed isotropically and acoplanarly with more than three jets in the final state, then the C shape parameter is close to 1. Hence for this analysis, this quantity is especially useful to separate the $q\bar{q}$ background from the signal.

Cut 5: Jets must have at least two Tracks

This helps to reduce the number of background events with isolated leptons or photons.

Cut 6 to 8: Convergence of Kinematic Fits

In the preselection, three different kinematic fits are required to converge, i. e. to have a χ^2 probability exceeding 10^{-5} at least for one of the six possible assignments of jet pairs to the Higgs and the Z^0 boson. Those are

- a four constraint fit,
- a 5.5 constraint fit,
converging for at least one jet pairing found by this fit
- a five constraint fit,
that is required to converge for at least one jet pairing according to both the five constraint fit and the 5.5 constraint fit.

Cut 9: Ratio of the Matrix Elements for Higgs-strahlung and WW Production

The matrix elements were chosen in accordance to 5.1.3. Events were considered as background, if the logarithms of the Higgs-strahlung matrix element and of the WW matrix element differed by more than -9 . This corresponds to a ratio of the matrix elements of roughly 10^{-4} .

5.3 The Likelihood Selection

5.3.1 The Likelihood Ratio Method

The likelihood procedure makes simultaneous use of a number of variables, rather than cutting with respect to each single variable. This method is suitable when a clear distinction between signal and background in a single variable is not possible, and a probabilistic approach is of more use.

The binned distributions of each variable are normalized to unity for all three event classes, hence they directly yield a probability density for an event belonging to each class. The joint probability densities for all variables are calculated, and their values for the three event classes are compared by the *Likelihood Ratio*

$$\mathcal{L} = \frac{\prod P_i(\text{signal})}{\sum_{sg,2f,4f} \prod P_i}, \quad (5.8)$$

considering all i variables and summing over the signal Monte Carlo (sg) and the simulation of both background classes ($2f$ and $4f$).

Then a cut is applied at the likelihood value which optimizes the analysis regarding efficiency and purity. This is quantified in a *Figure of Merit* (c. f. [51]). The remaining data events are considered as candidates.

5.3.2 Likelihood Variables

The likelihood discriminant is built of seven variables, mainly matrix elements, to make an efficient use of the kinematic properties of the final state topologies.

Energy Difference of the Jets

The four momenta of the jets are taken from a fit with four constraints. The energies of the jets are compared, and the difference is taken between the jets with the highest and the lowest energy. This variable reaches larger values for both background classes, due to the smaller "boost" of the Higgs events.

Kinematic Fit for WW Events

A kinematic fit is applied, forcing the four vector of at least one jet combination to be compatible with the measured center of mass energy. In addition, both jet pairs must be equal to the mass of the W boson for this jet combination. The χ^2 probability of this fit serves as likelihood variable.

Matrix elements

Three matrix elements enter the likelihood variable:

- *The EXCALIBUR matrix element for QCD as described in 5.1.3.*
It reaches slightly higher values for Higgs-strahlung than for the four fermion background. For quark pair events it reaches considerably higher values, thus providing a good discrimination power.
- *The ratio of the matrix element of WW events and Higgs-strahlung.*
This variable already served as a cut in the preselection. Its distribution is much broader for background events. It further enhances the discrimination to the four fermion background, as the according distribution peaks at slightly lower values, reflecting the larger WW matrix element for those events.
- *The matrix element of Higgs-strahlung after a soft 5.5 constraint fit.*
For the hZ channel it reaches its maximum at higher values than for both background classes. As was shown in [46], those two matrix elements are only slightly correlated. This is interpreted as coming from the dominance of the WW matrix element in the first variable.

Number of Tracks in the Detector

This variable uses the total number of tracks that an event leaves in the detector. It was added to enhance the sensitivity to $h \rightarrow gg$. A gluon leaves more low momentum tracks when it passes the detector than do quarks. Hence this variable reaches higher values for Higgs events with gluons in the final state. For four fermion events, it does not discriminate between signal and background.

5.3.3 Figure of Merit

The cut value of the resulting Likelihood-distribution is determined such that it optimizes the analysis performance. According to [51], a Figure of Merit is defined

$$FoM = \frac{2.1 * \sqrt{B + 2.04}}{\epsilon} \quad (5.9)$$

which reaches its minimum when the efficiency ϵ is high, with the number of remaining background events B being small. The parameters account for the differences between Gaussian and Poisson distributions in the case of small event numbers. With this procedure, an optimal working point can be found, including luminosity information, but being independent of the (a priori unknown) signal cross section.

5.3.4 The Likelihood Cut

According to equation 5.8, the likelihood values were calculated for the Monte Carlo distributions of each event class. A cut value of around 0.6 proved on average to have the best Figure of Merit for all test masses, therefore only events with a likelihood exceeding 0.6 were kept. Data events with at least such a likelihood were chosen to be candidates.

Chapter 6

Results of the Analysis

This analysis used approximately 210 pb^{-1} of data recorded with the OPAL detector in the year 2000. The center of mass energy ranged from 202 to 209 GeV, with a luminosity weighted center of mass energy of 206.1 GeV.

The results were interpreted within the framework of 2HDM and for a model assuming a confinement phase in the electroweak sector (c. f. 2.3.2). Neither approach found a signal of a Higgs boson but did help to increase the lower mass bound.

Different decay modes of the Higgs boson were considered, with gluons and quarks in the final state. For the fermionic decays Higgs Monte Carlo simulations were used that consisted only of charm quark events and of the mixture of decays as predicted by the Standard Model, respectively. In the latter, the predominant mode is the decay into bottom quarks (about 80 %). An overview of the samples is given in appendix A.

In order to provide a single analysis for all different decay modes, one final state had to be chosen for the reference histograms to build the likelihood discriminants. The choice that provided the best efficiency for all three modes proved to be the Standard Model mixture, which was therefore taken for the analysis within the 2HDM interpretation. Unless specified, the results presented in this chapter refer to this case.

For the alternative interpretation in the framework of a confined Higgs phase, the reference histograms with gluon final states were taken, as this is the only major decay mode to which this analysis is sensitive.

Fig. 6.9 compares the efficiencies after the likelihood selection for the different signal types at different test masses. The keys are given in the caption. The black curves are the smoothed distributions. The different efficiencies show that the analysis is almost, but not entirely flavour independent. Therefore the lowest curve was chosen for the further procedure, being the efficiency for gluon decays.

The efficiencies reach a maximum for test masses of around 110 GeV for all signal types. This is due to a number of effects: Events with a low

| Cut | data | total background | two fermion background | four fermion background | efficiency in % for $m_H = 100$ GeV |
|-------------------|-------|------------------|------------------------|-------------------------|-------------------------------------|
| (1) | 18400 | 17981.1 | 13843.1 | 4138.0 | 99.9 |
| (2) | 6500 | 6490.5 | 4011.4 | 2479.1 | 97.8 |
| (3) | 2200 | 2176.2 | 497.2 | 1679.0 | 93.6 |
| (4) | 2164 | 2095.5 | 436.0 | 1659.5 | 93.6 |
| (5) | 1999 | 1927.0 | 409.5 | 1517.5 | 91.9 |
| (6) | 1766 | 1736.4 | 358.8 | 1377.6 | 90.4 |
| (7) | 1692 | 1665.2 | 327.3 | 1337.9 | 89.6 |
| (8) | 422 | 405.8 | 87.5 | 318.3 | 63.2 |
| (9) | 393 | 386.1 | 85.9 | 300.2 | 62.8 |
| (\mathcal{L}) | 59 | 57.5 | 10.3 | 47.2 | 23.3 |

Table 6.1: Cutflow table for an assumed mass of the Higgs boson of 100 GeV. The number of selected events after each cut is given, the numbering refers to the description in chapter 5.2.1. Cuts (1) to (7) are valid for all test masses. Cut (8), (9) and the Likelihood Cut (\mathcal{L}) are given for an assumed Higgs mass of 100 GeV. The efficiency is indicated for a Higgs boson mass of 100 GeV with a gluon final state using the reference histograms for Standard Model decays. The procedure is explained in the text.

Higgs mass lose more energy by initial state radiation, therefore they are more likely to be cut away by the preselection cuts using \sqrt{s} and the four constraint fit [45]. The maximum in fig. 6.9 is further enhanced by the test mass dependent preselection cuts and the likelihood discriminant. This reflects the better discrimination power of the variables when the Higgs mass is assumed to differ more from the masses of the background bosons.

The performance of the cuts is shown in table 6.1. The number of data events after each cut is compared with the number of expected background events. The cuts are numbered as in 5.2.1. Data and background simulations are in good agreement throughout the analysis. The efficiency is given for the detection of a Higgs boson with a mass of 100 GeV that decays into a gluon pair.

Fig. 6.2 to 6.5 show the likelihood input variables (except for the number of tracks) for low test masses (60 GeV) and high test masses (110 GeV). The tracknumber will be examined separately. All plots are normalized to surface unity.

Fig. 6.2 and 6.3 represent the decay of a Higgs boson according to the Standard Model. Not only the explicitly test mass dependent variables, such as the 5.5C fit matrix element provide a better distinction in the case of high masses, but also for example the difference of the jet energies (fig. 6.1).

The distributions for a two gluon decay are shown in fig. 6.4 for a low test mass of 60 GeV and in fig. 6.5 for a test mass near the kinematic limit

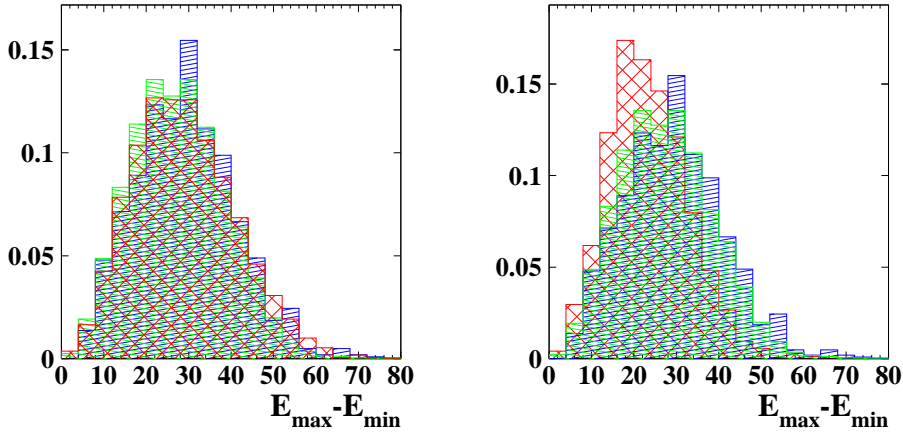


Figure 6.1: The energy difference of the highest and the lowest energetic jet. On the *left* the distributions are shown for a mixture of test masses between 80 and 110 GeV. The plot on the *right* shows the energy difference for a test mass of 100 GeV. The blue distribution represents the four fermion background, the green distribution the two fermion background, and the red one the signal distribution, respectively.

of 115 GeV. The differences are rather small for most variables, but can be seen for example in the 5.5 C-fitted matrix element for hZ events, where the signal reaches higher values for the gluon final state. The distributions for the two background classes are identical in both cases.

In fig. 6.6 a likelihood input variable is shown that yields a good discrimination power for gluon events (lower part, see also section 5.3.2). This is the overall number of tracks that an event leaves inside the detector. For quark pair final states, the overlap of signal and background histograms is almost complete. Therefore this variable does not enhance the performance of the analysis with respect to 2HDM. This is the main reason for the more distinct likelihood distributions in case of a two gluon decay of the Higgs boson with respect to the Standard Model.

The likelihood distributions for a number of test masses from 60 GeV to 115 GeV are shown in fig. 6.7 and in fig. 6.8. The histograms are normalized to the luminosity of the data. Events were considered as candidates if their likelihood exceeded 0.6.

The black histograms indicate the signature of a Standard Model Higgs boson (fig. 6.7) and of a Higgs boson decaying to gluons exclusively (fig. 6.8). The green histograms represent the two fermion background, the yellow histograms show the four fermion background, respectively. The data is given by the dots. Data and background are in agreement.

Both modes have in common that the sensitivity is higher for high test

masses, when the kinematic properties of Higgs bosons and the background are more different, due to the higher mass difference.

In fig. 6.10 the number of candidates is shown as a function of the test mass. The maximum at around 75 GeV is due to W bosons, whose one component is forced to the Z mass. The second W boson then has a reconstructed mass which is below its original value [45]. There is a small excess for test masses between 98 GeV and 108 GeV. This is supposed to come from a background fluctuation, because none of the according data events has a likelihood value exceeding 0.8. The biggest discrepancy occurs for a hypothetical Higgs mass of 98 GeV and has a significance of 1.78 standard deviations.

SM Higgs signal, $m_H = 60 \text{ GeV}$

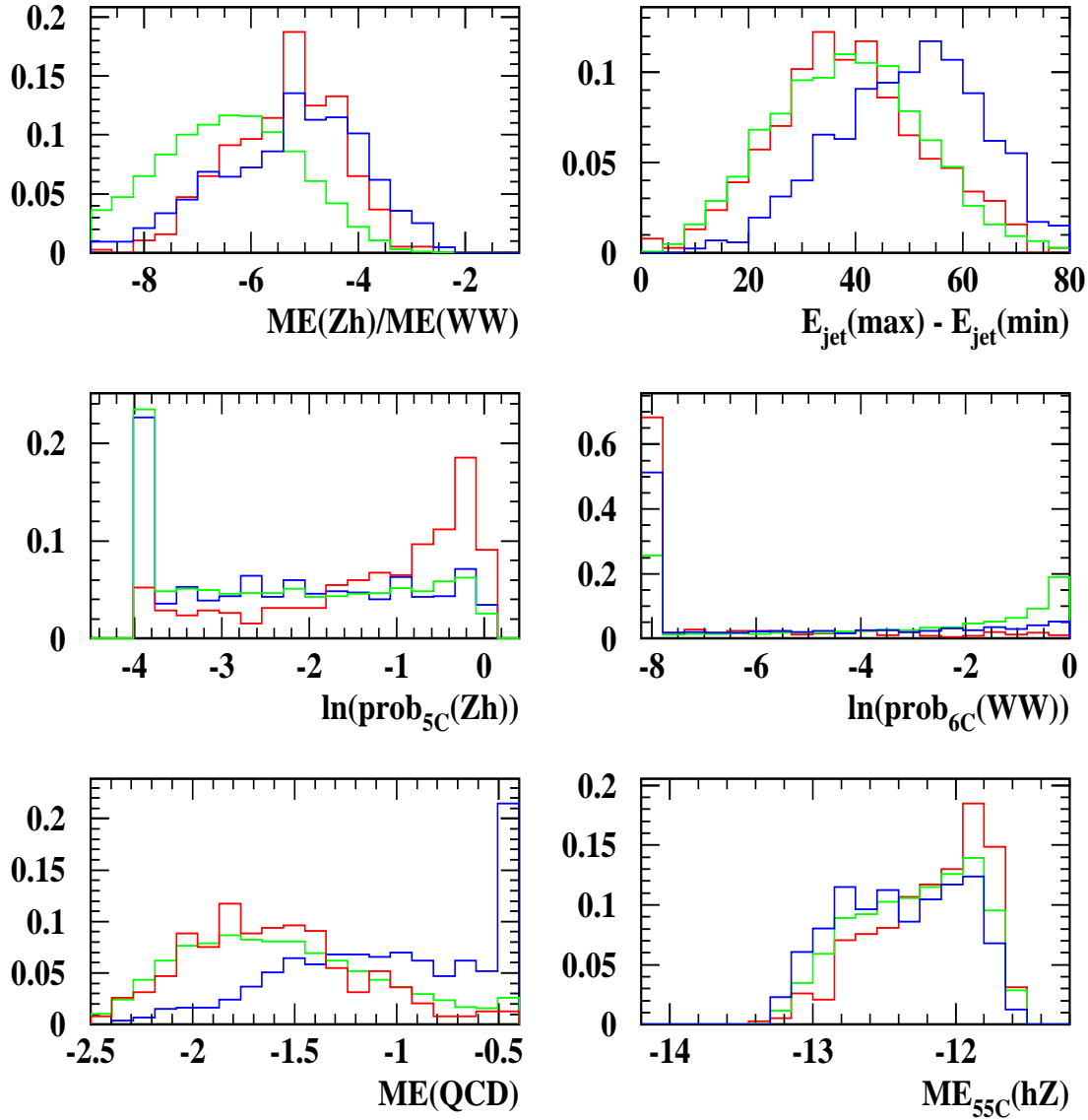


Figure 6.2: The likelihood variables for Higgs bosons with decays as in the Standard Model. The blue histogram represents the four fermion background while the red and the green histograms show the distributions for the expected Higgs signal and the two fermion background. The test mass dependent variables are chosen for a hypothetical Higgs mass of 60 GeV. This mass was the lowest under consideration.

SM Higgs signal, $m_H = 110$ GeV

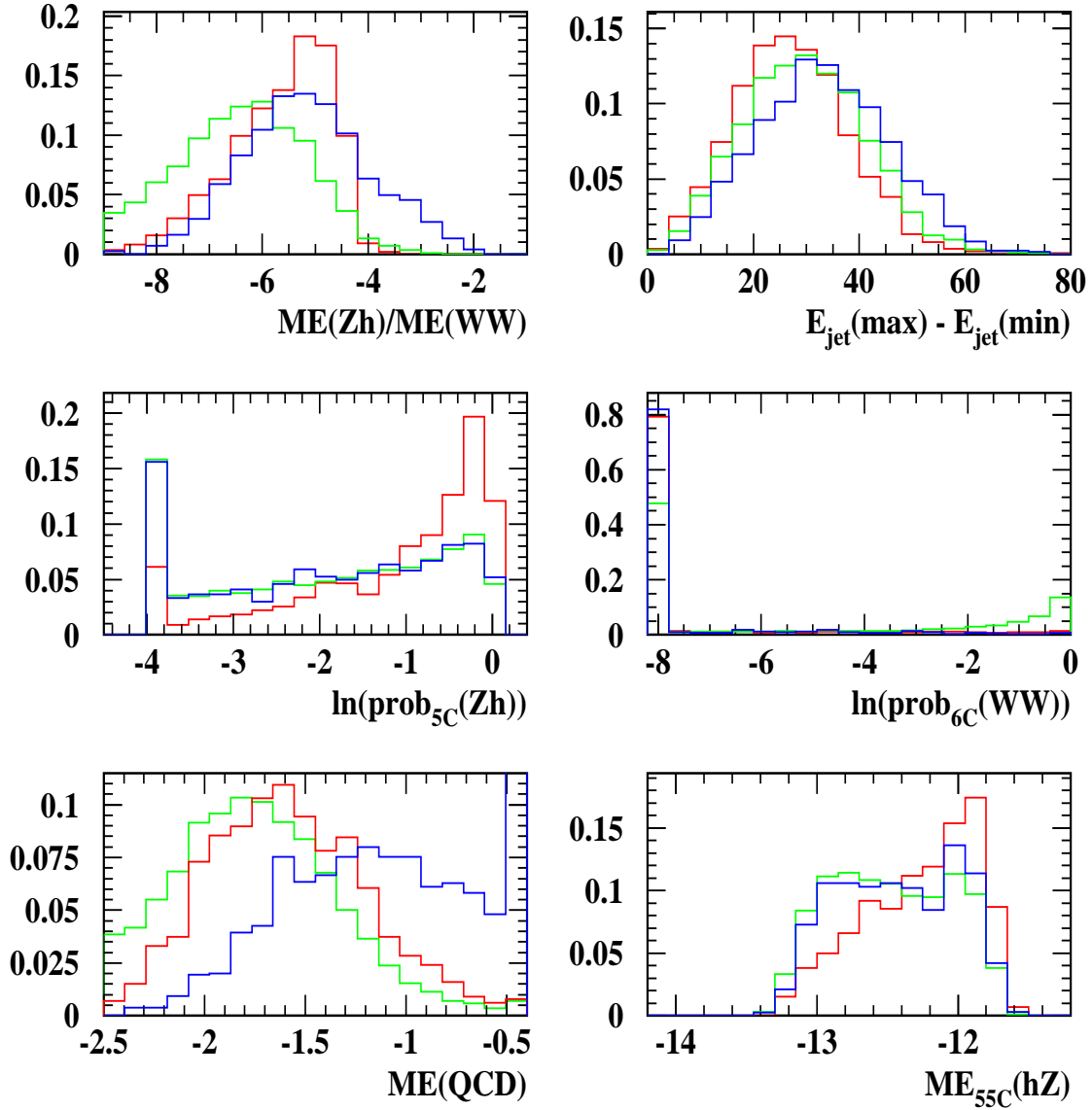


Figure 6.3: This figure shows again the likelihood input variables for Standard Model decays, but now for a test mass of 110 GeV, that is about 5 GeV below the kinematic limit. The keys are the same as before.

$H \rightarrow gg, m_H = 60 \text{ GeV}$

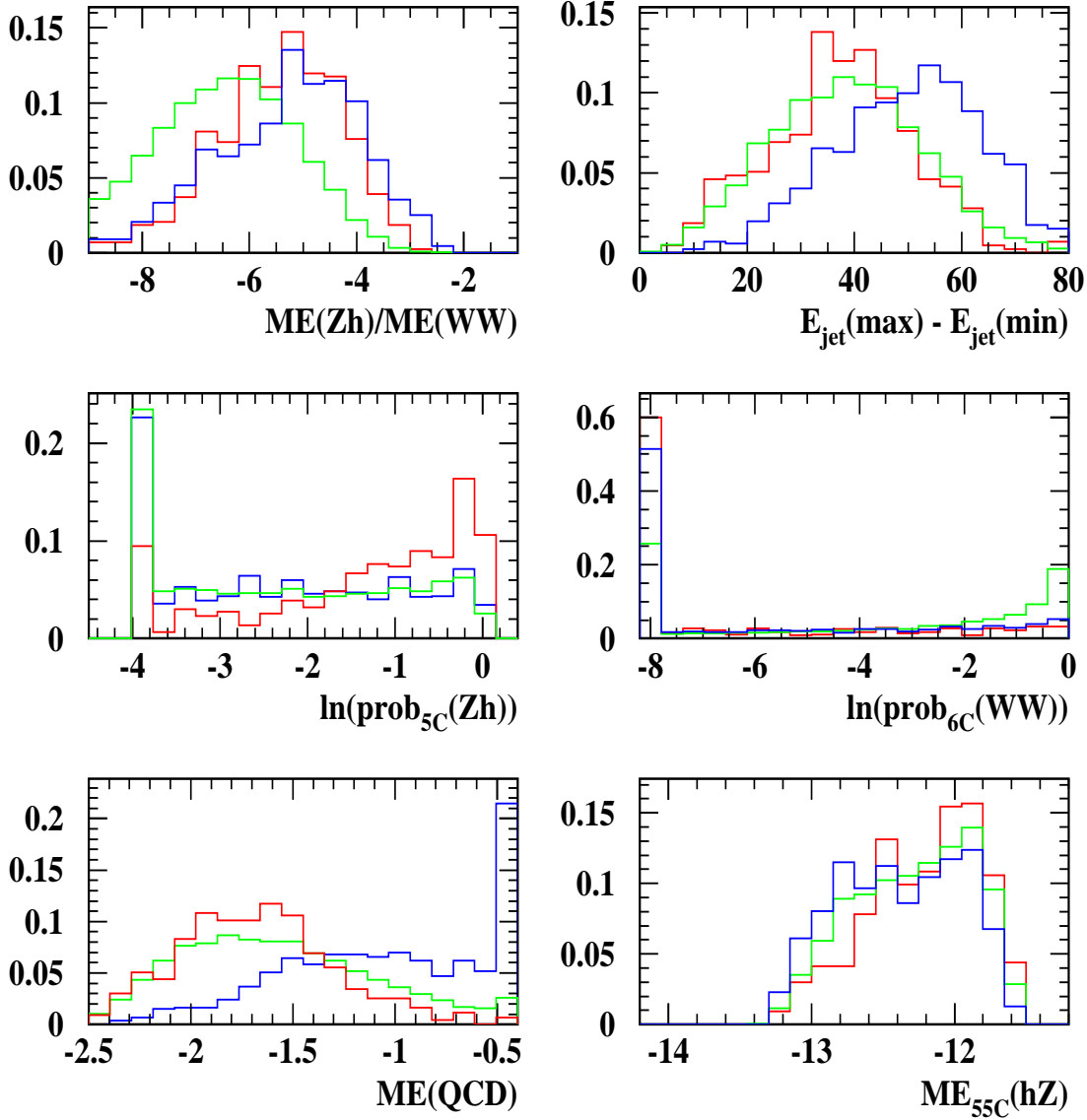


Figure 6.4: Likelihood input variables for the Higgs boson decaying into gluon pairs. The Higgs mass is assumed to be 60 GeV. The blue histogram shows the distributions for the four fermion background, while the red and the green histograms represent the Higgs signal and the two fermion background, respectively.

$H \rightarrow gg, m_H = 110 \text{ GeV}$

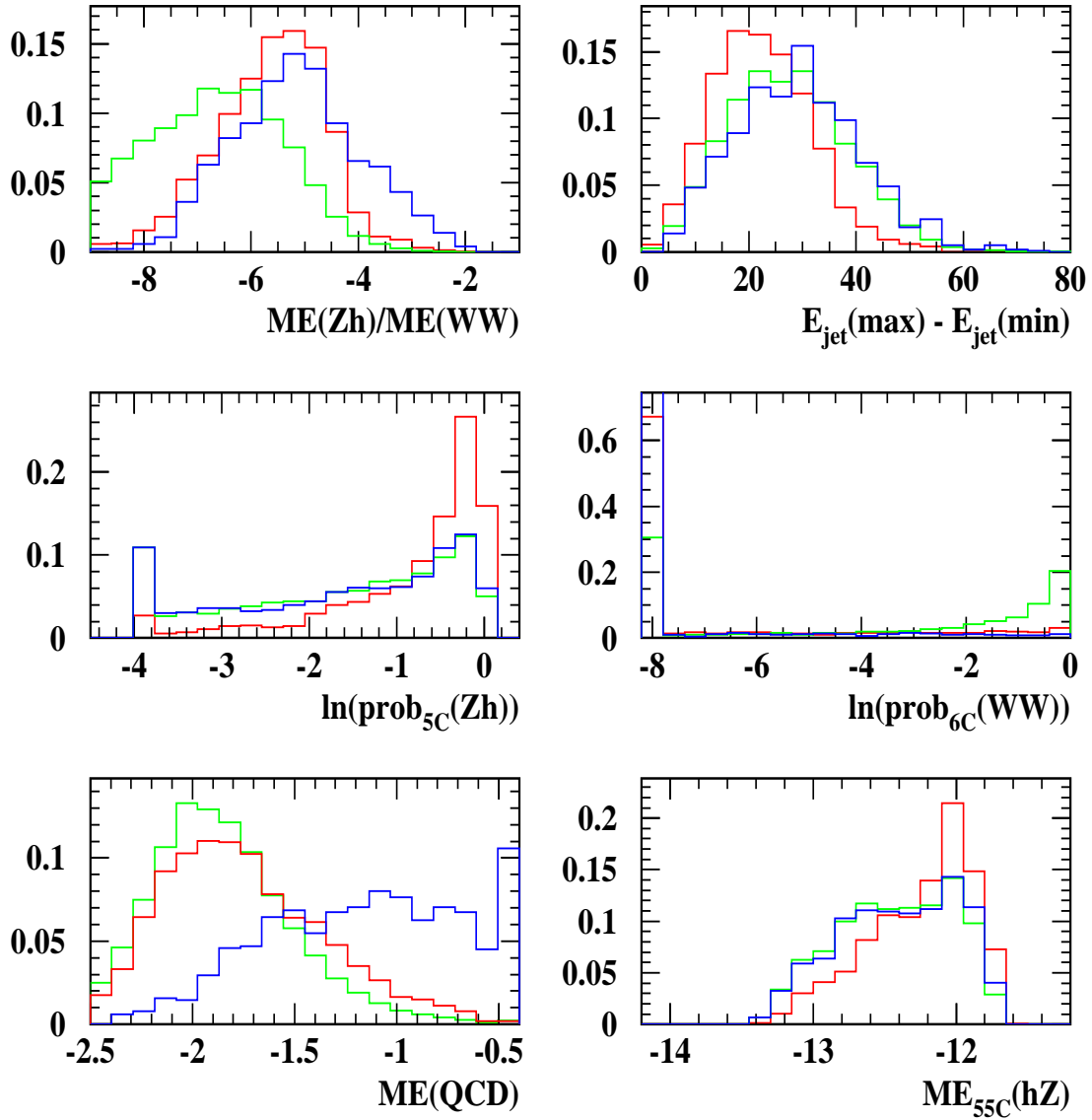


Figure 6.5: The same decay mode as in the previous figure, but for a Higgs mass of 110 GeV. As in the case of Standard Model decays, the discriminating power increases with mass.

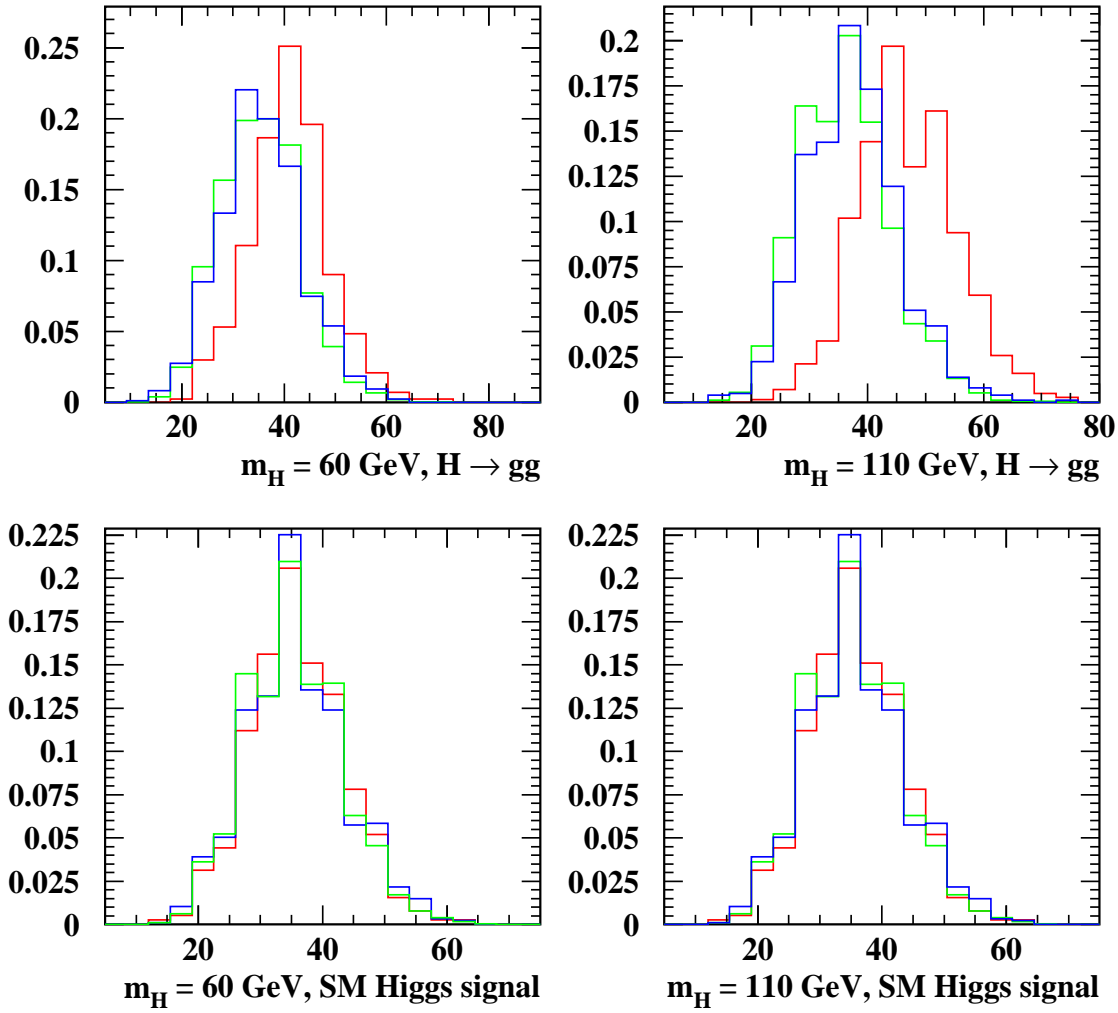


Figure 6.6: The different behaviour of the "number of tracks" variable, that is described in 5.3.2. The blue reference histograms show the four fermion background, the green and the red histograms the two fermion background and the signal simulations, respectively. It is obvious that this variable yields a good discrimination power for gluon final states throughout the mass range and especially for high test masses. For decays of the Higgs boson into quark pairs on the other hand it does hardly provide any discrimination.

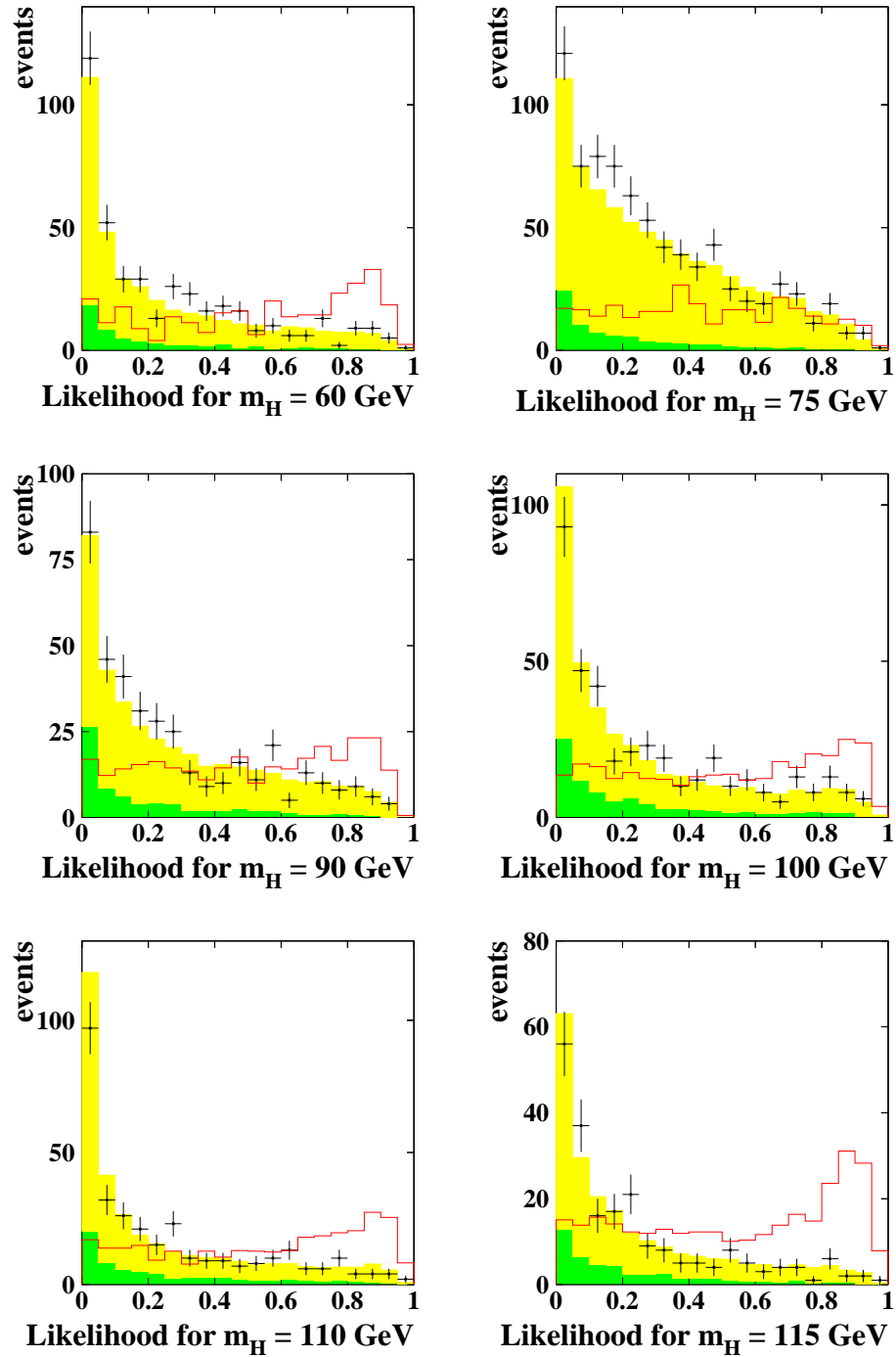


Figure 6.7: Likelihood distributions for hypothetical Higgs boson masses between 60 and 115 GeV. The dots represent the distributions for the data including the statistical error. The green and yellow histograms represent the four fermion and the two fermion background, respectively. The red histogram shows the likelihood distribution for $h \rightarrow c\bar{c}$, using the reference histograms for the Standard Model decay mixture. The normalisation of the Higgs signal is arbitrary, the other distributions are normalized to the data luminosity. A description of the features can be found in the text.

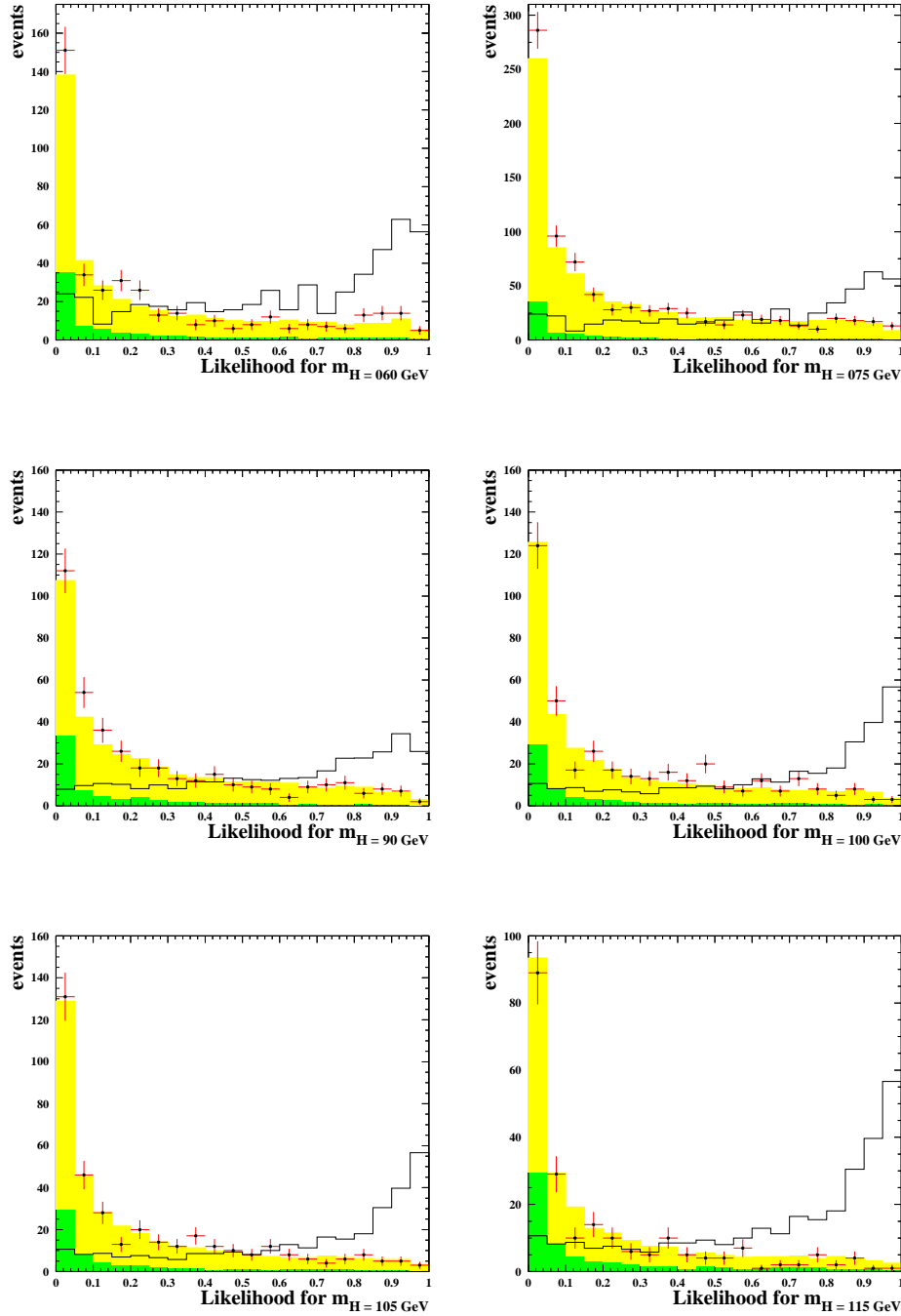


Figure 6.8: Likelihood distributions for the same test masses as before, but using the reference histograms as obtained by the $h \rightarrow gg$ samples. The green and yellow histograms represent the four fermion and the two fermion background, respectively. The dots indicate the data, and account for the statistical error. The red histogram shows the likelihood distribution for the gluon final state. The normalisations are the same as before. A comparison with fig. 6.7 shows that the analysis is more sensitive to gluons if one uses gluon final states for the reference histograms. This mainly comes from the track number variable.

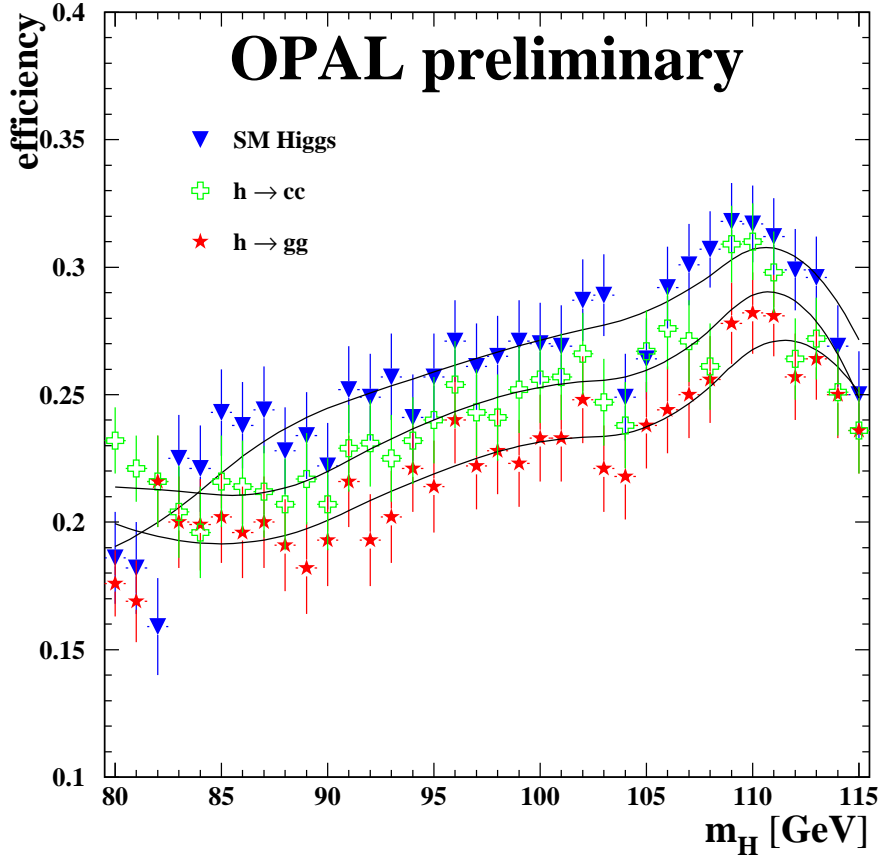


Figure 6.9: Efficiency of the likelihood selection as a function of m_H determined from different Monte Carlo samples. The dots represent the efficiency obtained from the same samples with Standard Model branching ratios which also define the reference histograms at each test mass. The stars, crosses and triangles correspond to independent samples where the Higgs boson decays exclusively to gluon pairs, $c\bar{c}$ pairs or to the Standard Model decay mixture, respectively. For the limit calculation (c.f. 8.1) the efficiencies have been fitted separately (smooth curves) and the smallest of the three is taken at each mass point.

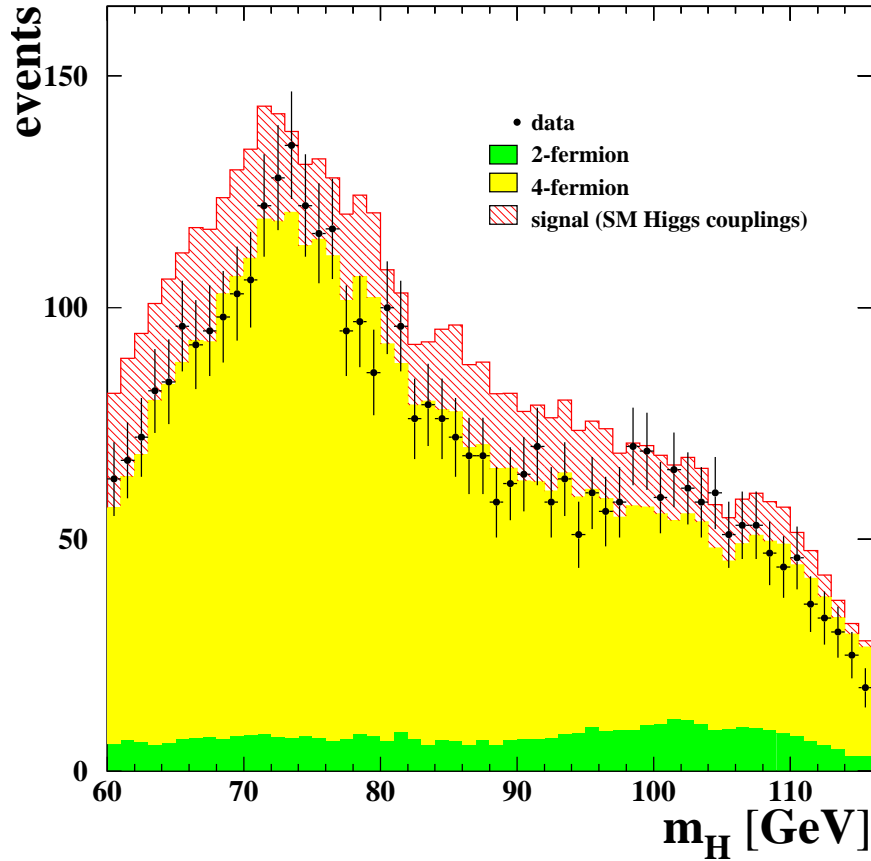


Figure 6.10: The number of events recorded in the year 2000 that pass the likelihood selection for test masses between 60 GeV and 115 GeV. The number of data events are indicated as dots with the statistical errors, the green and the yellow histograms correspond to the number of events expected from the two fermion and the four fermion background, respectively. The possible contribution from a Higgs boson with a mass equal to the test mass, assuming Standard Model cross sections, is shown in the hatched histogram. All distributions have been normalized to the luminosity of the data. The shape of the distributions is discussed in the text.

Chapter 7

Uncertainties and Systematics

Not only statistical fluctuations contribute to the total error of an analysis, but also uncertainties due to imperfections of the experimental setup and the analysis tools. Especially the modelling of the experimental outcome by using Monte Carlo simulations leads to systematic errors that must be examined in detail.

Several types of errors were studied for this analysis, including the influence of the different center of mass energies in the data. Mismodelling of the variables was considered, as well as the differences between Monte Carlo generators. The procedure follows [52] and [53], except for the study of the different center of mass energies. The details for the latter are given below.

If Monte Carlo Higgs events were needed to calculate the errors, then the Standard Model samples were used. The errors are supposed to be uncorrelated. Therefore the square root of the sum of the errors squared is given as the combined error if not explicitly stated otherwise.

7.1 Sources of Systematic Uncertainties

7.1.1 Monte Carlo Dependence

The entire analysis was done with Monte Carlo events obtained by additional event generators. For the four fermion background the EXCALIBUR generator was used instead of GRC4F, for the two fermion background PYTHIA replaced KK2F. As the only available Higgs event generator was HZHA, the signal Monte Carlo distributions could not be studied.

In order to derive the error due to the chosen hadronisation scheme, samples were examined that used the HERWIG generator instead of the JETSET package. For each Monte Carlo simulation the variation in the number of the selected events was obtained. The results were scaled to the relative

| | 85 GeV | 100 GeV | 115 GeV |
|--------------|--------|---------|---------|
| PYTHIA | 5.12 % | 12.75 % | 8.4 % |
| GRC4F/HERWIG | 2.4 % | 1.00 % | 2.5 % |
| EXCALIBUR | 10.4 % | 9.60 % | 2.5 % |

Table 7.1: The errors that were obtained when using alternative Monte Carlo Simulations. All errors are given for assumed Higgs boson masses of 85, 100 and 115 GeV.

contribution of each background class to the total background expectation. The errors are given in table 7.1 for a number of Higgs masses.

7.1.2 Different Center of Mass Energies

The data that was obtained with the OPAL detector in the year 2000 was not taken at one single center of mass energy \sqrt{s} but in a range from 200 GeV to almost 209 GeV (c. f. fig. 4.4) with a luminosity weighted mean of 206.1 GeV. This is important for the present analysis because the variables strongly depend on the available kinetic energy, being the difference between the center of mass energy and the hypothetical Higgs mass: $\sqrt{s} - m_H$. Varying the test mass by a few GeV can change the efficiency of the selection by several percent as can be seen in fig. 6.9.

This effect is softened, though, because 85 % of the data were taken at (206 ± 1) GeV, the center of mass energy that was assumed for this analysis. Only a small amount of data was obtained at different center of mass energies (table 7.2). Thus, the resulting errors are lowered. They were examined in detail for test masses between 95 and 105 GeV, leading to errors of less than 2.5 %. Some of the values are given in table 7.4 for the background estimation and in table 7.5 for the efficiency.

The modelling of the variables was also studied by a comparison between the Monte Carlo events and the data (c. f. section 7.1.4). All data was used with the actual center of mass energy. Therefore the errors described in this section will not be included into the final error.

| 202 GeV | 204 GeV | 206 GeV | 208 GeV |
|---------|---------|---------|---------|
| 1.49 % | 9.45 % | 85.02 % | 4.11 % |

Table 7.2: The center of mass energy of the year 2000 data, given in bins of 2 GeV around the indicated values. The 202 GeV amount comprises all data at or below 203 GeV, the 208 GeV column all data at or above 207 GeV. By far the biggest amount can be found at around 206 GeV.

7.1.3 Test Mass Assumptions

The mass dependent variables are calculated for test masses between 60 and 115 GeV with a step width of 1 GeV. The Monte Carlo events were generated in steps of 5 GeV. Even though both widths are within the order of the width of the Z boson, they lead to an additional error that was calculated by doing the analysis with different mass assumptions around an actual mass of 105 GeV. An interpolation between the masses then yields the error in the efficiency. Using mass assumptions between 100 and 110 GeV for a 105 GeV Standard Model Higgs boson sample, an error of 0.64 % per GeV test mass was obtained.

7.1.4 Mismodelling of the Variables

Uncertainty also arises from a mismodelling of the variables in the Monte Carlo event generators. The resulting error was derived following a procedure proposed in [53]. The mean values of the distributions in the data and the Monte Carlo event classes were calculated and each variable in each Monte Carlo simulation was scaled by the ratio of the means $\langle \text{data} \rangle / \langle \text{Monte Carlo} \rangle$. Then the analysis was repeated using the scaled values. The difference between the expected backgrounds using either the original or the scaled variables yields the measure for the systematic uncertainty. The total error on the background was obtained by weighting the uncertainty for the two background classes with its contribution to the total background.

The errors resulting from this procedure are given in table 7.3. They are bigger than the errors given for data and simulations at a center of mass energy of 189 GeV [45]. This can be explained with the rather complex spectrum of center of mass energies in the year 2000 data, while all Monte Carlo simulations were optimized for a center of mass energy of 206 GeV.

| | 85 GeV | 100 GeV | 115 GeV |
|------------------|--------|---------|---------|
| total background | 7.59 % | 6.02 % | 5.55 % |
| efficiency | 7.2 % | 6.33 % | 5.2 % |

Table 7.3: Uncertainties due to mismodelling of the variables in the Monte Carlo event generators. For the error in the efficiency the Standard Model Higgs boson samples are used. Both errors are given for Higgs mass assumptions of 85 GeV, 100 GeV and 115 GeV.

This effect would lead to decreasing errors as the hypothetical Higgs masses increase, because only data events at high center of mass energies (206 GeV, 208 GeV) contribute to the candidate events. This decrease indeed was observed, and it can be seen in table 7.3 for the errors in both background classes and in the efficiency.

7.2 Final Errors

By far the biggest error contribution comes from the use of different Monte Carlo generators. With a slight dependence of the assumed mass of the Higgs boson, they sum up to a total error of around 10 %. In table 7.1 they are given explicitly for each event generator and for a number of mass hypotheses. The second largest contribution comes from errors in the modelling of the variables, as can be seen in table 7.3. The biggest errors are obtained for small mass assumptions. The error due to statistical fluctuations is given in the last line of table 7.4 for the background estimation and in table 7.5 for the efficiency.

The first line (\sqrt{s} refers to the explicit study of errors due to the different center of mass energies. These uncertainties are not included into the total errors, because they are already considered with the error resulting from the mismodelling of the variables (c. f. 7.1.4).

| | 85 GeV | 100 GeV | 115 GeV |
|----------------|---------|----------|---------|
| \sqrt{s} | 0.942 % | 1.73 % | 1.79 % |
| Monte Carlos | 11.85 % | 11.52 % | 9.11 % |
| Variables | 7.59 % | 6.05 % | 5.55 % |
| Σ | 14.07 % | 13.012 % | 10.67 % |
| Stat. Fluct 2f | 0.77 % | 0.77 % | 0.77 % |
| Stat. Fluct 4f | 2.31 % | 2.31 % | 2.30 % |
| Total Error | 14.76 % | 13.24 % | 10.95 % |

Table 7.4: Overview of the systematic errors of the background estimation as obtained with the above procedures. The last line gives the total error.

| | 85 GeV | 100 GeV | 115 GeV |
|--------------|--------|---------|---------|
| \sqrt{s} | 1.31 % | 1.31 % | 1.31 % |
| Variables | 7.2 % | 6.33 % | 5.2 % |
| Test Masses | 0.64 % | 0.64 % | 0.64 % |
| Fluctuations | 2.23 % | 2.20 % | 2.23 % |
| Total Error | 7.56 % | 6.73 % | 5.69 % |

Table 7.5: The considered systematic errors of the efficiency, as obtained for the Standard Model Higgs samples. The errors are given for Higgs boson masses of 85, 100 and 115 GeV.

Chapter 8

Interpreting the Results

8.1 Deriving a Limit

As already mentioned, no significant excess of data events with respect to the Monte Carlo estimations could be found with this analysis.

On the other hand, data and background do not completely agree. Therefore a measure has to be found how well the observed events are compatible with the hypothesis that they are exclusively due to the Standard Model background processes.

This is done by the means of *confidence levels* [54, 55]. The *confidence interval* is defined to be the range $[x_-, x_+]$ around the hypothetical value of a continuous random variable x , in which a certain fraction of events lie. The confidence level is then given as the probability that the observed value is at least as far away as observed from the most probable outcome of the assumed probability density function:

$$Prob(x_- \leq x \leq x_+) = \int_{x_-}^{x_+} P(x) dx \quad (8.1)$$

According to this definition, confidence levels can be given for the presence of only background events (CL_B), or for a mixture of signal and background events (CL_{S+B}). Frequently the 95 % confidence level is stated.

The Higgs searches at the LEP experiments use a slightly different definition of confidence levels to estimate whether an observed outcome is due to the pure background hypothesis or to the additional presence of a signal. The procedure accounts for background fluctuations in the case of a small signal, but a high background rate [55]:

$$CL = 1 - \frac{CL_{S+B}}{CL_B} \quad (8.2)$$

Since here the "background only" hypothesis will be tested, this means that a signal can be excluded for a given mass and parameter range with a certain

confidence level. The highest mass thus excluded is called the *confidence limit*.

Furthermore, *observed* and *expected* confidence limits must be distinguished. The observed confidence limit refers to the outcome of the actual experiment, while the expected confidence limit is defined as the expectation value of the observed limit, given that an experiment can be repeated many times. This is done by Monte Carlo studies. The expected confidence level for the background hypothesis is defined to be $\langle CL_b \rangle = 0.5$ in the case of a pure background sample. The expected limit for the signal exclusion ($1 - \langle CL_s \rangle$) yields a measure for the sensitivity of an analysis.

Signal and background events are distinguished by a discriminator called *test statistics*. It yields the main difference between the limit setting procedures. Here the mass of an event is used in the following way, according to [54, 55]:

First, a hypothetical mass is attributed to the Higgs boson. Then a weight X_{ki} is assigned to each event i in each channel k by

$$X_{ki} = \frac{D_k(m_i - m_{theo})}{D_{k,max}} \quad (8.3)$$

$D_k(m_i - m_{theo})$ gives the expected spectrum of reconstructed particle masses, under the assumption of a correct mass hypothesis. Its maximum $D_{k,max}$ is reached at k, max . Furthermore, the different channel sensitivities and signal to background ratios are accounted for by scale factors c_k .

Finally, the test statistics is defined as the scaled sum of the event weights:

$$X = \sum_k c_k \sum_i X_{ki} \quad (8.4)$$

The probability distribution of the weight sum then allows one to derive the confidence limit. This is done on the basis of the obtained events (obeying Poisson statistics) and the channel weights, c_k . A detailed description can be found in [54].

This procedure leads to a predicted number of *observed* and *expected candidates*, $N95_{obs}$ and $N95_{exp}$, respectively. They yield the number of the observed and the expected candidates within the 95 % confidence level. These event counts can be transformed into a limit on the cross section σ_{95} within the 95 % confidence level by

$$\sigma_{95} = \frac{N_{95}}{\sum_k \epsilon_k BR_k \mathcal{L}_k} \quad (8.5)$$

with the branching ratios BR_k , the efficiency ϵ_k and the Luminosity \mathcal{L}_k summed over all k search channels. N_{95} can either be $N95_{obs}$ or $N95_{exp}$, leading to a $\sigma_{95_{obs}}$ or a $\sigma_{95_{exp}}$, respectively.

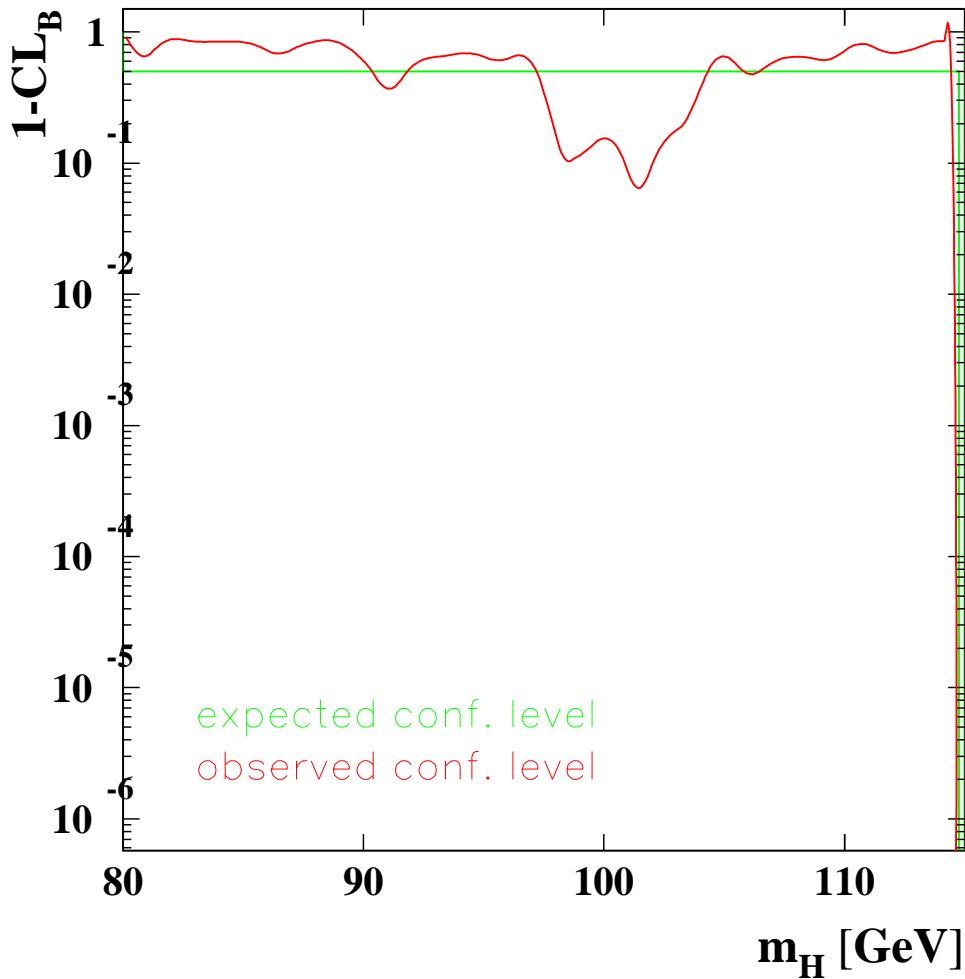


Figure 8.1: $1 - CL_B$ is given for a range of test masses between 80 and 115 GeV. The green and the red line indicate the expected and the observed confidence level, respectively. The minimum at around 100 GeV reflects the excess in the observed number of candidates. It is well above the 5σ excess that is required to claim a discovery. Such an excess corresponds to a $(1 - CL_B)$ of $\sim 5.7 * 10^{-7}$, corresponding to the bottom of the plot.

8.2 General Flavour Independent Limits

In fig. 8.1 $(1 - CL_B)$ is given for a range of test masses between 80 and 115 GeV. Given that all values are close to 1 this result sustains the above assumption that no new particle was found with this analysis. The observed confidence level reaches a minimum for Higgs masses between 100 and 105

GeV. This reflects the excess in fig. 6.10. If one wanted to claim a discovery, an excess of 5σ would be needed, which is equivalent to $(1 - CL_B) \sim 5.7 * 10^{-7}$. This value defines the bottom of the figure.

For a most general flavour independent interpretation, no *a priori* information is given about the branching fractions of the Higgs boson. The Higgs boson is thus assumed to only have hadronic decay modes. In fig. 8.2 the cross sections are therefore given in terms of the Standard Model cross sections of the Higgs boson, $BR(H^0 \rightarrow \text{hadrons}) * k^{95}$. k^{95} scales the indicated cross sections to the cross sections of a Standard Model Higgs boson: $k^{95} = \frac{\sigma_{fl.ind.}}{\sigma_{SM}}$. Assuming $k^{95} = 1$, one obtains an expected lower mass limit for the Higgs boson of $m_{min,exp} = 99.75$ GeV and an observed minimal mass of $m_{min,obs} = 97.5$ GeV, except for a small non excluded region between 90.5 GeV and 91.5 GeV. The discrepancy between the observed and the expected limit at Higgs masses of around 100 GeV comes mainly from the candidate excess that was shown in fig. 6.10.

8.3 Limits within 2HD Models

The interpretation within the framework of 2HD Models is very similar to the general flavour independent case. The main difference are the lower bounds for the hadronic branching fractions of the 2HDM Higgs boson with respect to the Standard Model. These are given in fig. 8.3, as well as the Standard Model cross sections in the presented range of Higgs masses.

Since the Higgs boson decays hadronically with a branching fraction of more than 90 % if its mass does not exceed 101 GeV, the above mass limits with respect to the Standard Model are unchanged, the main differences arise at Higgs masses above 101 GeV, when the contributions of the hadronic decay modes loose their importance in the 2HDM.

On the other hand, more concise statements can be made in an interpretation within 2HD Models: The hadronic branching fraction is known, therefore a range of production cross sections can be excluded. The process under study is the Higgs-strahlung, which is proportional to $\sin^2(\beta - \alpha)$ (c. f. section 3). The mass range up to 97.5 GeV can be excluded for a $\sin^2(\beta - \alpha) = 1$, except for Higgs masses between 90.5 and 91.5 GeV. For Higgs masses above this value, no statement can be given, as $\sin^2(\beta - \alpha) \leq 1$ must be assured anyway.

8.4 Combining the OPAL Channels

If one wants to provide a search that is sensitive to all possible final states emerging from a hadronically decaying Higgs boson, cases must be considered where the Z boson decays leptonically. The present analysis is not sensitive to these modes.

Four leptonic search channels can be distinguished, according to the decay mode of the Z boson:

- the neutrino (“missing energy”) channel
- the tau channel
- the electron channel
- the muon channel

OPAL data with center of mass energies from 189 GeV onwards has been analysed with flavour independent searches in all leptonic channels and in the here discussed four jet channel [56, 35]. A number of channels have also been studied at lower energies [35]. Especially for Higgs boson masses below ~ 60 GeV, analyses from the first run of LEP (LEP1) with center of mass energies of ~ 91 GeV lead to better limits. For masses on the order of the Z boson width (~ 5 GeV) and below, model independent approaches are more sensitive [35].

A combined limit can be obtained in analogy to the procedure described in section 8.1 by accounting for the different efficiencies and luminosities of the channels. The branching ratios are given by the Standard Model branching fractions of the Z boson.

Again a limit was obtained for the general flavour independent case and in the framework of Two Higgs Doublet Models (upper and lower part of fig. 8.5, respectively). They should be interpreted in an analogous way to the figures presented in sections 8.2 and 8.3.

The mass up to which the flavour independent searches are sensitive to branching ratios below the Standard Model predictions are 107.3 GeV, as given by the expected limit (green line in the upper part of fig. 8.5), and 105.3 GeV within 2HDM (green line in the lower part of the figure). The observed limit is in both cases lower, being 101.8 GeV for the flavour independent interpretation and 99.7 GeV within the Two Higgs Doublet Models.

The discrepancy between the expected and the observed limit is due to two effects. First the presented preliminary results do not include detailed systematic studies, so the systematic errors are estimated and include a certain safety margin. Second the excess in the four jet channel (as shown in fig. 8.2 and fig. 8.4) is also present in the combined results, even though it is partially cancelled by a deficit in the missing energy channel.

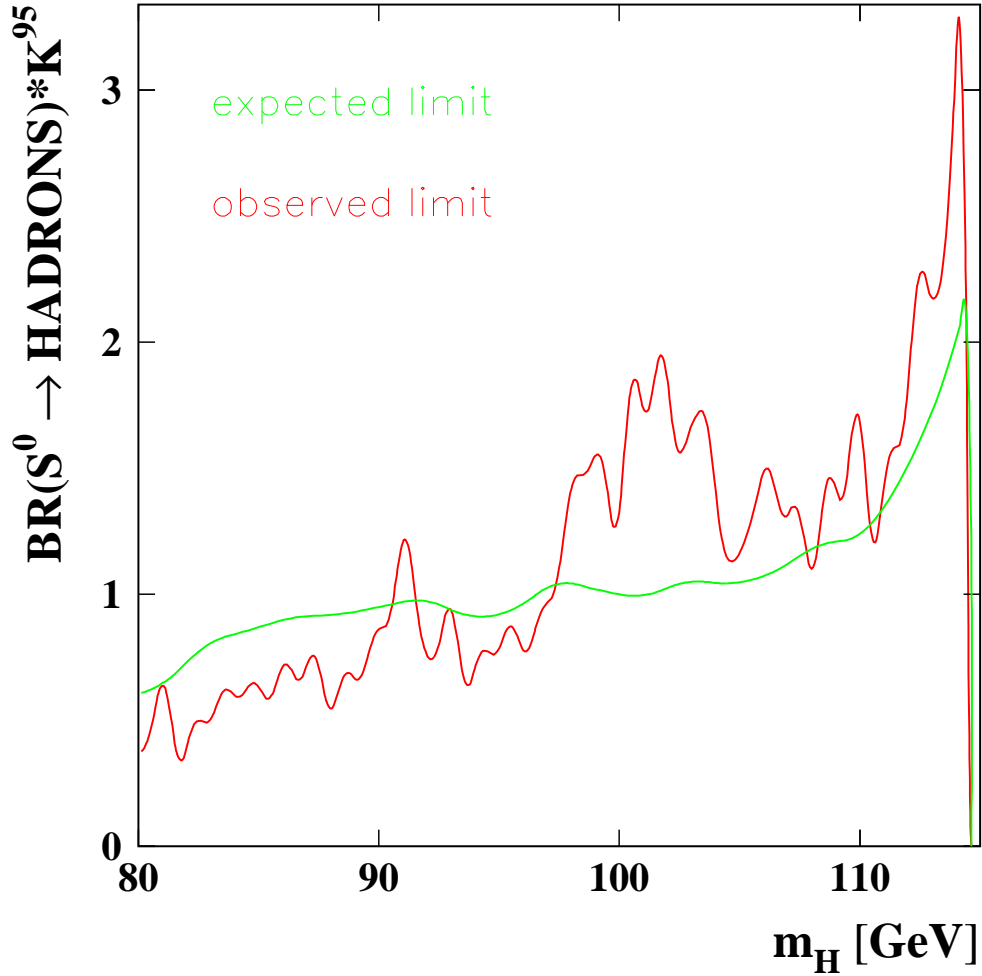


Figure 8.2: The excluded cross sections with respect to the Standard Model Higgs boson versus Higgs masses between 80 GeV and the kinematic limit. A value of 1 on the vertical axis is obtained for Standard Model cross sections. The excluded areas lie above the red line for the observed limit and above the green line for the expected limit. Masses below 97.5 GeV can be excluded on a 95 % Confidence Level for cross sections up to the Standard Model values, except for $90.5 \text{ GeV} < m_H < 91.5 \text{ GeV}$. The vertical axis refers to S^0 instead of H^0 . This indicates that this analysis is general enough to allow statements about any scalar neutral boson, given that only the kinematic properties are used.

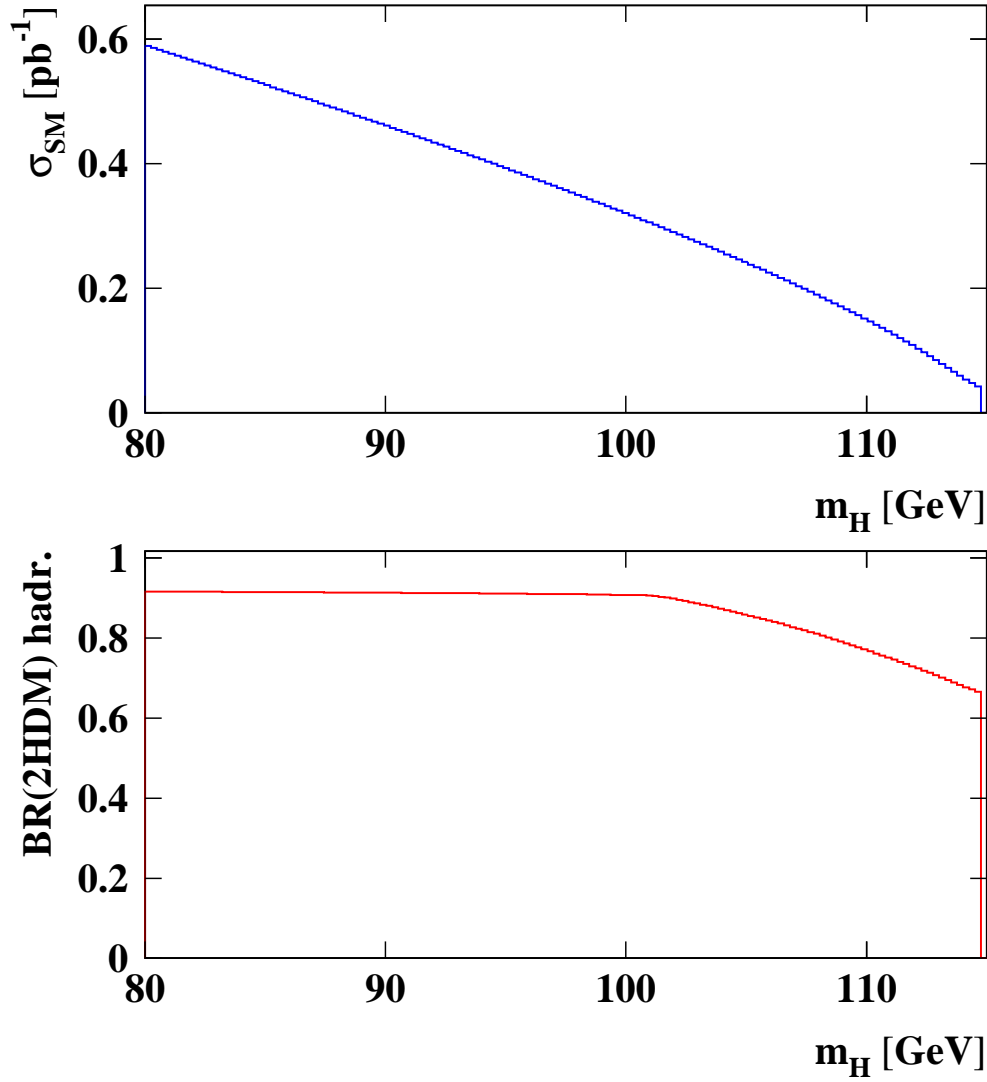


Figure 8.3: Standard Model cross sections and minimal branching fractions for Higgs-strahlung in 2HDM. *upper part*: The Standard Model cross sections for Higgs bosons in the studied mass range. Their rapid decrease, together with the excess at around 100 GeV, are the main reasons that this analysis can exclude Higgs bosons with branching fractions below the Standard Model values only up to 97.5 GeV, which is about 17 GeV below the kinematic limit. *lower part*: The minimal branching fractions for Higgs-strahlung in 2HDM. Up to a Higgs boson mass of 101 GeV, this is the main production process with a frequency of around 90 %. For masses above this value the branching fraction decreases considerably while the associated production of h and A bosons increases (c. f. section 3).

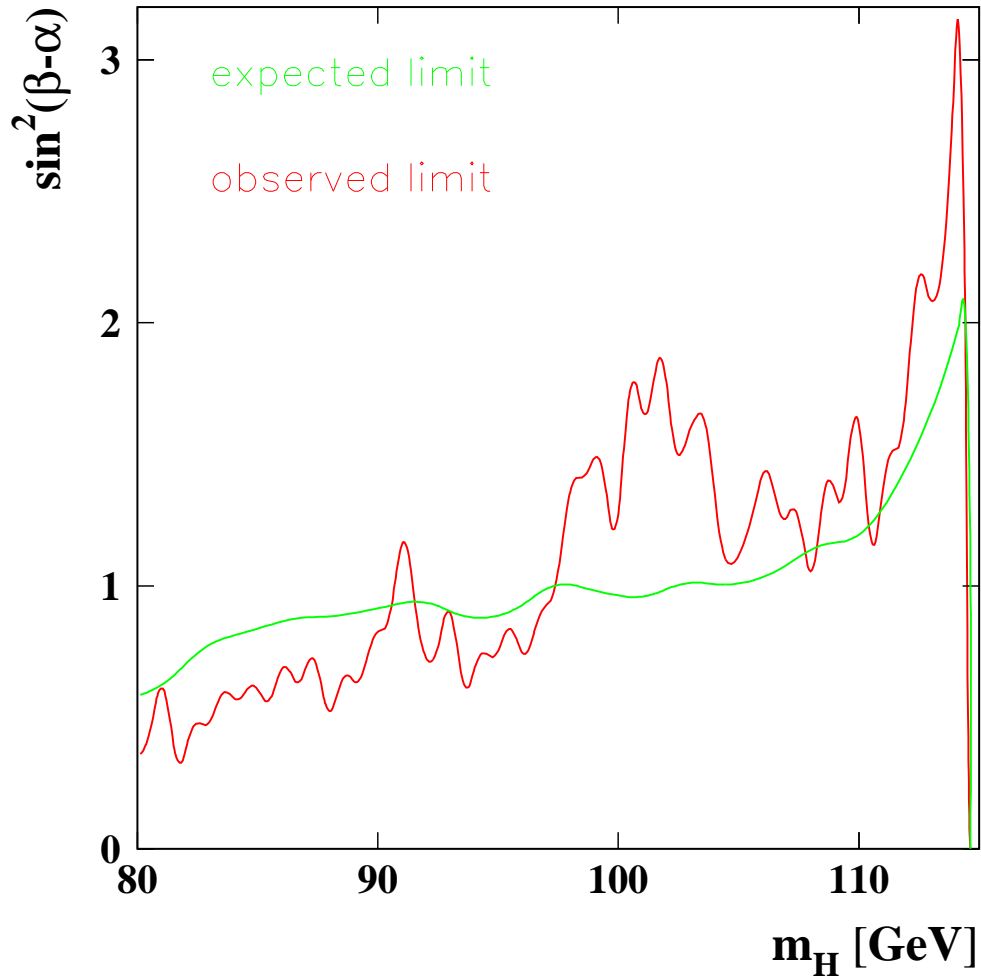


Figure 8.4: The expected limit (green line) and the observed limit (red line), accounting for the minimal production cross section in 2HD models. The main difference arises for Higgs masses above 101 GeV, when the cross section for Higgs strahlung decreases with increasing masses. (c. f. fig. 8.3)

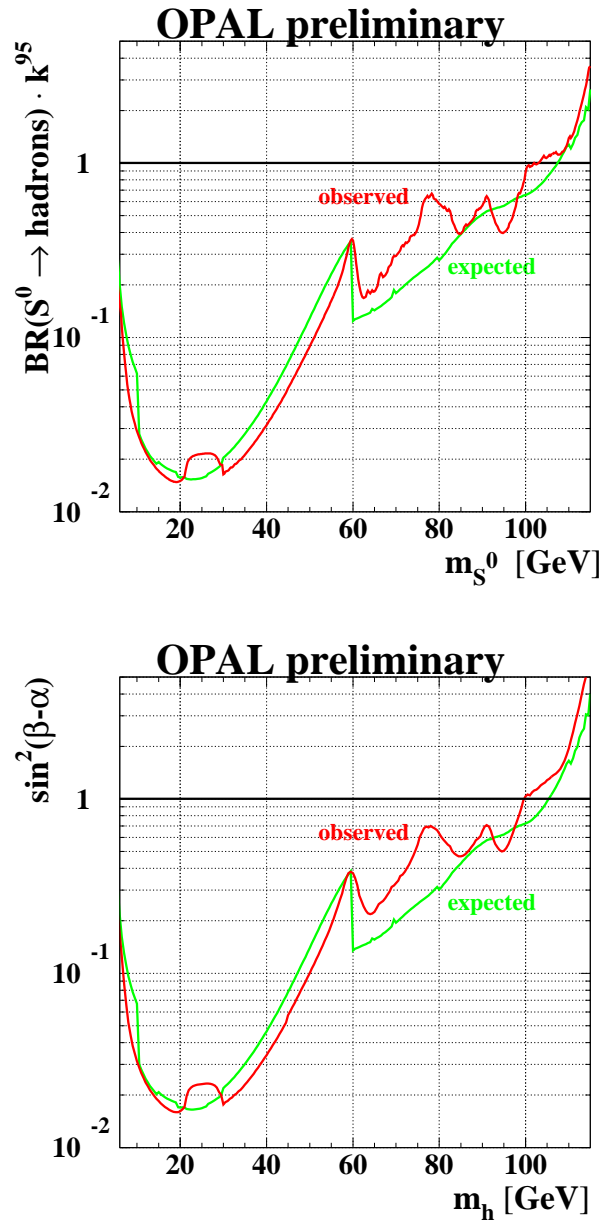


Figure 8.5: *upper part*: The observed limit (red line) and the expected (green line) in the general flavour independent search as obtained by combining all OPAL data with center of mass energies from 91 GeV to 209 GeV in the available channels. For very low Higgs masses (up to 5 GeV), a model independent approach has been used. As before the branching ratios for a neutral scalar boson are given in terms of the Standard Model branchings. All possible Higgs masses are considered up to 115 GeV. For Higgs masses below 60 GeV, LEP1 analyses were taken, the jump at 60 GeV comes from the not optimal mapping of the two regions. *lower part*: The analogous limits for the 2HDM interpretation.

| | $m_H=90$ GeV | $m_H=95$ GeV | $m_H = 100$ GeV | $m_H=105$ |
|--------------------------------|--------------|--------------|-----------------|-----------|
| H \rightarrow gg | 90.9 % | 85.24 % | 76.54 % | 64.13 % |
| H \rightarrow $\gamma\gamma$ | 3.43 % | 3.2 % | 3.06 % | 2.57 % |
| H \rightarrow WW | 5.14 % | 10.0 % | 18.51 % | 30.59 % |
| H \rightarrow ZZ | 1.04 % | 1.37 % | 1.89 % | 2.71 % |

Table 8.1: Branching fractions for a composite Higgs boson as predicted in [21, 57]. The strong coupling constant α_s was chosen to be $\alpha_s = 0.119$.

8.5 Limits for a Composite Higgs Boson

In chapter 2.3.2 a model was introduced that assumes the Standard Model Higgs boson to be a bound state of fundamental bosons. Its production cross sections are unchanged with respect to a fundamental Standard Model Higgs boson, but the spectrum of possible final states is entirely different. Decays to fermions do not occur. Therefore the contributions of other channels grow, most of all for gluon final states.

An overview of the predicted decay channels and their abundances can be obtained from table 8.1. For Higgs boson masses above the threshold of W pair production the branching fractions into gluons decrease rapidly while the WW contribution grows. This analysis is not sensitive to W pair production, therefore limits will be given only for parts of the kinematically accessible range.

The final state branching fractions within this composite model depend to a high degree on the strong coupling constant α_s . Its value has been measured only to a low precision, it is at present $\alpha_s = 0.118 \pm 0.002$. As before it is therefore useful to give limits on the branching fractions rather than on the cross sections, that are valid only for a specific parameter choice.

The result is shown in fig. 8.6, where the limit is given in terms of the total Standard Model branching fractions to hadrons. The value of α_s will influence the factor k^{95} that yields the relative abundance with respect to the Standard Model. The observed limit (red line) and the expected limit (green line) are calculated under the assumption that the Higgs boson only decays to gluons. Higgs bosons in composite models can be excluded up to a mass of 98.75 GeV (observed limit) and up to 106.5 GeV (expected limit) if their gluon branching fraction equals the hadronic branching fraction in the Standard Model. Again there is a big discrepancy between the observed and the expected limit. As before this can be mapped to the excess at mass hypotheses of around 103 GeV (fig. 6.10).

If one considers specific branching fractions including information about α_s , then cross section limits can be given as shown in fig. 8.7. The hadronic branching fraction of the Z boson is assumed to be 69.89 % as in the Standard Model, α_s is chosen to be 0.119. This value leads to comparably low

branching fractions for gluons. The cross sections are given in pb and as a function of the hypothetical Higgs boson mass. Again the difference is mainly attributed to the above mentioned excess. The blue line gives the cross section as predicted by the model. Composite Higgs bosons can be excluded if their mass does not exceed 97.5 GeV using only this search channel and the OPAL data taken in the year 2000. A combination with other channels could significantly enlarge the excluded region. This applies to final states where the Higgs boson decays into gluons and the Z boson into leptons, but also to the other decay channels of the Higgs boson. Furthermore the sensitivity could be enhanced by a combination with analogous searches of the other three LEP collaborations.

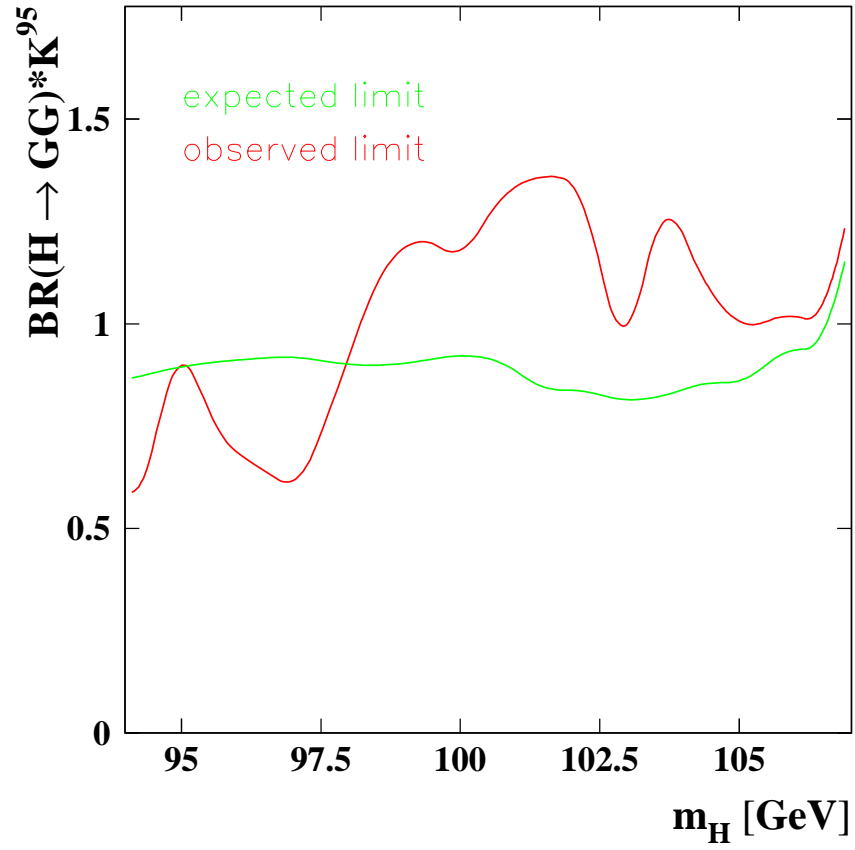


Figure 8.6: Exclusion limits on a 95 % Confidence Level if only Higgs boson decays into gluons are considered. The branching fractions are given in terms of the total hadronic branching fractions in the Standard Model. The green line shows the expected limit, the red line refers to the observed limits. A branching fraction is excluded for a specific mass assumption if it is above the line.

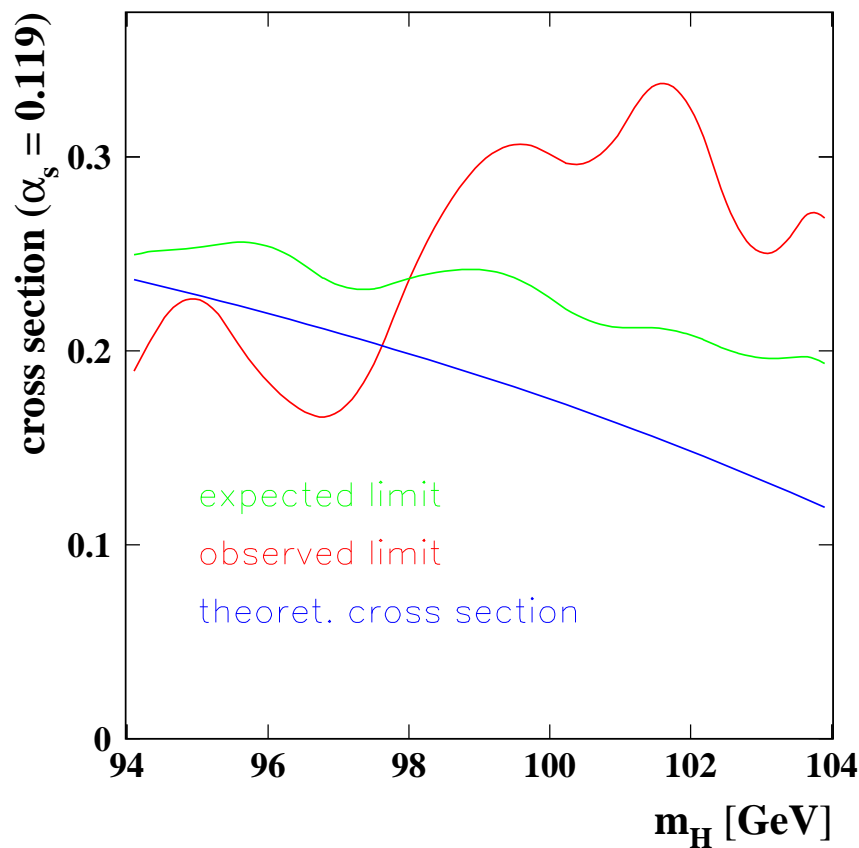


Figure 8.7: Cross section limits for a composite Higgs boson that decays predominantly into gluons. The cross sections are given in pb and as a function of the hypothetical Higgs mass. The blue line gives the predicted cross sections for a strong coupling constant $\alpha_s = 0.119$. Composite Higgs bosons are excluded if their mass does not exceed 97.5 GeV (observed limit). A combination with other channels is recommended to enhance the excluded region.

Chapter 9

Summary and Outlook

A search for the Higgs boson was presented that was applied to the full data taken in the year 2000 with the OPAL detector at the highest LEP energies and with an effective center of mass energy of 206.1 GeV. The analysis did not make use of one of the most common and efficient features of Higgs searches, being the explicit measurement of secondary vertices ("b tagging"), but was purely based on kinematic properties. Such a *flavour independent* approach has a lower sensitivity with respect to other Higgs boson searches but its results are valid for interpretations within a number of extensions of the Standard Model.

This refers especially to the class of *Two Higgs Doublet Models* that predict five different physical Higgs bosons, in contrast to the Standard Model with only one Higgs field doublet and one measurable Higgs particle. The preferred decay into b quarks, the main prerequisite for the b tagging in the Standard Model searches, is not necessarily valid within 2HDMs.

Here it was searched for the lightest scalar 2HDM Higgs boson produced in the Higgs-strahlung process: $e^+e^- \rightarrow Z^* \rightarrow hZ$. The analysis focused on events with a four jet topology in the final state, with both the Higgs and the Z boson decaying either into quarks or gluons.

The abundance of the production process can be lowered with respect to the Standard Model due to a possible competitive process, the associated production of the lightest scalar Higgs boson together with a massive pseudoscalar, the A boson. The relative frequency of the two mechanisms is not known.

Another possible theoretical framework is given by models that assume the electroweak bosons to be composite objects. In the studied mass range they predominantly decay into gluons, depending on the details of the theory. Since this is one of the final states covered by this analysis, a statement about this theory could be made as well.

No Higgs boson was found in the data for any of the theoretical assumptions. Therefore exclusion limits for a 95 % confidence level were given as a

function of the branching fraction and with respect to the hadronic branching fractions in the Standard Model. The general flavour independent limit obtained with only this search channel is 97.5 GeV, if one assumes the minimal branching fractions as predicted by Two Higgs Doublet Models. The Higgs boson was supposed to only decay into hadrons. Masses between 90.5 GeV and 91.5 GeV could not be excluded at a 95 % Confidence Level with only this channel.

If the Higgs boson only decays into gluons with the hadronic Standard Model branching fractions, then Higgs bosons could be excluded with a mass below 98.75 GeV. Accounting for the cross sections in the presented Composite Model this leads to a minimal Higgs boson mass of 97.5 GeV.

The analysis technique makes explicit use of mass hypotheses. This enhances its sensitivity in two ways. Some of the studied variables cannot be defined without assuming a specific Higgs boson mass and all variables allow a clearer discrimination between signal and background when given for a well defined mass rather than a range of masses. Physically two main features were used for the distinction: the mass of the Higgs boson and the isotropy of its final state.

The main background arises from the production of W and Z pairs (*four fermion background*), but also from quark pair production (*two fermion background*). W and Z bosons are vector particles and therefore do not decay isotropically. Quark pairs decay in a pencil like shape due to the conservation of their four momentum. On the contrary, the Higgs boson is a scalar particle and should have a spheric symmetric final state.

After a cut based preselection, a likelihood function is constructed that allows the simultaneous consideration of seven variables. These include matrix elements and fit probabilities assuming several kinematic constraints. Data events were considered as candidates when they exceeded a threshold value that was chosen to maximize the sensitivity of the selection.

It might be possible to enhance the sensitivity of this analysis by a few percent with an interpolation between the center of mass energies and the test masses. This is presently being studied. Furthermore the limit can be improved by including the systematics as described in chapter 7.

Combining the results of different search channels and of the four LEP experiments is a way to enlarge the excluded regions. The OPAL search channels have been combined for the 2HDM interpretation and for the general flavour independent limit. A combination with the other LEP experiments is presently being done.

In addition, this analysis can be used for some parameter regions in the Minimal Supersymmetric Model – at present the most popular way to extend the Standard Model – where the decay into b quarks is strongly suppressed. This will be done in the near future.

For a composite Higgs boson, no combined limit has been given so far. Combining this gluon specific search with the other flavour independent

channels, but also including the so called fermiophobic Higgs searches with $h \rightarrow \gamma\gamma$, could lead to significant progress, either by enlarging the excluded region, or by finding some first hints of the Higgs boson. Searches for WW final states are not performed at OPAL because the signatures of the signal and the background final states are almost identical.

A Standard Model Higgs discovery at LEP will not be made, as the accelerator and its detectors are being dismantled. The search for the Higgs boson will go on, but it is very unlikely that it will immediately lead to new results. Several years will pass until the experiments at Fermilab's Tevatron collider and CERN's planned LHC complex will be able to provide enough data for major progress. The race between the two is on the horizon. Especially the LHC will cover the whole possible mass range in the Standard Model Higgs boson. This is also the case for most of the parameter ranges in the alternative theories. Once the Higgs boson is detected, its properties can be studied at one of the next linear colliders, as they are planned now at different locations. And if no Higgs boson can be found, then nature might provide new and unexpected phenomena to discover.

So everyone knows about mass except for particle physicists? This is still true. But we keep on working.

Appendix A

List of Monte Carlo Simulations

– TWO FERMION BACKGROUND –

| Generator | Run | gen. Events | Luminosity | Process |
|---------------------|------|----------------|-------------------------|----------------------------------|
| KK2F 4.01: | 5193 | 250,000 events | 3146.2 pb ⁻¹ | $Z, \gamma \rightarrow q\bar{q}$ |
| <i>Systematics:</i> | | | | |
| PYTHIA 6.125: | 5135 | 150,000 events | 1993.0 pb ⁻¹ | $Z, \gamma \rightarrow q\bar{q}$ |

– FOUR FERMION BACKGROUND –

| Generator | Run | gen. Events | Luminosity | Process |
|----------------------------|-------|-------------|-----------------------|--|
| GRC4F 2.1: | 10071 | 44870 | 5000 pb ⁻¹ | $Z, \gamma \rightarrow q\bar{q}q\bar{q}$ |
| | 10070 | 47015 | 5000 pb ⁻¹ | $Z, \gamma \rightarrow q\bar{q}l^+l^-$ |
| | 10075 | 191143 | 5000 pb ⁻¹ | $Z, \gamma \rightarrow q\bar{q}e^+e^-$ |
| <i>Systematics:</i> | | | | |
| EXCALIBUR 011/04: | 10351 | 96600 | 1000 pb ⁻¹ | $Z, \gamma \rightarrow \text{any 4 f}$ |
| | 10352 | 10700 | 1000 pb ⁻¹ | $Z, \gamma \rightarrow \text{any 4 f}$ |
| GRC4F 2.1: (HERWIG 5.9) | 10961 | 47015 | 5000 pb ⁻¹ | $Z, \gamma \rightarrow q\bar{q}ll$ |
| | 10962 | 44870 | 5000 pb ⁻¹ | $Z, \gamma \rightarrow q\bar{q}q\bar{q}$ |

– HIGGS BOSON SIGNAL MONTE CARLOS –

| Generator | Run | gen. Events | Masses | Process | |
|-------------------------|-------------------------|---------------|---------------|--------------------------|----------------|
| HZHA 3.03: | | | | | |
| ($\sqrt{s} = 206$ GeV) | 10196 | 1000 per mass | 60 - 79 GeV | SM Higgs boson | |
| | 10109 | 2000 per mass | 80 - 115 GeV | SM Higgs boson | |
| | 10327 | 1000 per mass | 60 - 79 GeV | $h \rightarrow gg$ | |
| | 10697 | 4000 per mass | 80 - 115 GeV | $h \rightarrow gg$ | |
| | 10332 | 1000 per mass | 60 - 79 GeV | $h \rightarrow c\bar{c}$ | |
| | 10698 | 4000 per mass | 80 - 115 GeV | $h \rightarrow c\bar{c}$ | |
| <i>Systematics:</i> | | | | | |
| HZHA 3.03: | | | | | |
| ($\sqrt{s} = 202$ GeV) | 9616 | 2000 per mass | 80 - 115 GeV | SM Higgs boson | |
| | ($\sqrt{s} = 204$ GeV) | 10225 | 2000 per mass | 80 - 115 GeV | SM Higgs boson |
| | ($\sqrt{s} = 208$ GeV) | 10354 | 1000 per mass | 80 - 115 GeV | SM Higgs boson |

Bibliography

- [1] S. L. Glashow, J. Iliopoulos, and L. Maiani. Weak interactions with lepton-hadron symmetry. *Phys. Rev.*, D2:1285, 1970.
- [2] S. Weinberg. A model of leptons. *Phys. Rev. Lett.*, 19:1264–1266, 1967.
- [3] A. Salam and J. C. Ward. Electromagnetic and weak interactions. *Phys. Lett.*, 13:168, 1964.
- [4] H. Fritzsch, M. Gell-Mann, and H. Leutwyler. Advantages of the color octet gluon picture. *Phys. Lett.*, B47:365, 1973.
- [5] The LEP Collaborations and the LEP Electroweak Working Group. Combination procedure for the precise determination of z boson parameters from results of the LEP experiments. 2001.
- [6] R. P. Feynman. Space-time approach to quantum electrodynamics. *Phys. Rev.*, 76:769, 1949.
- [7] E. Fermi. An attempt of a theory of beta radiation. *Z. Phys.*, 88:161, 1934.
- [8] Particle Data Group. Review of particle physics. *European Physical Journal* **C15**, 2000.
- [9] C. Quigg. *Gauge Theories of the strong, weak and electromagnetic interaction*. Benjamin-Cummings, Reading (MA), 1983.
- [10] P. Schmöser. *Feynman Graphen und Eichtheorien für Experimentalphysiker*. Springer Verlag, 1995.
- [11] G. Ridolfi. An introduction to the standard model of electroweak interactions. Lecture Note, 2000.
- [12] R. Kleiss. Field theory for the standard model. Lecture Note, 2000.

- [13] G. 't Hooft. Dimensional regularization and the renormalization group. *Nucl. Phys.*, page 455, 1973.
- [14] P. Higgs. Broken symmetries and the masses of gauge bosons. *Phys. Rev. Lett.*, page 508, 1964.
- [15] J. Goldstone. Field theories with 'superconductor' solutions. *Nuovo Cimento*, page 154, 1961.
- [16] G. Kane. *Modern Elementary Particle Physics*. Perseus Books, Reading, MA, 1993.
- [17] F. Mandl and G. Shaw. *Quantenfeldtheorie*. Aula Verlag Wiesbaden, 1993.
- [18] J. F. Gunion, H. E.Haber, G. L.Kane, and S.Dawson. *The Higgs Hunter's Guide*. Addison-Wesley, Reading, MA, 1990.
- [19] Sheldon L. Glashow and Steven Weinberg. Natural conservation laws for neutral currents. *Phys. Rev.*, D15:1958, 1977.
- [20] X. Calmet and H. Fritzsche. The electroweak interactions as a confinement phenomenon. *Physics Letters B*, page 161, 2000.
- [21] X. Calmet and H. Fritzsche. The higgs boson might not couple to b quarks. *Physics Letters B*, 2000.
- [22] P. Igo-Kemenes. Searches for higgs bosons. *European Physical Journal C***15**, page 274, 2000.
- [23] T. Hambye and K. Riesselmann. Matching conditions and higgs mass upper bounds revisited. *Physical Review D***55**, page 7255, 1996.
- [24] Tatsuo Kawamoto. Standard model fit results. Talk given at the XXXVI Rencontres de Moriond, 2001.
- [25] P. Igo-Kemenes and the LEP Higgs Working Group. Status of higgs boson searches. Talk given at CERN, Nov. 3rd, 2000.
- [26] G. Cowan. *Statistical Data Analysis*. Oxford Univ. Press, 1998.
- [27] P. Ward and D. Ward. A GOPAL primer. unpublished, 1995.
- [28] Cern Program Library. Geant detector description and simulation tool. Long Writeup W5013, 1994.
- [29] Patrick Janot. Physics at LEP2. page 309, 1996. CERN 96-01.

- [30] J. Fujimoto et al. grc4f v1.1: a four-fermion event generator for e^+e^- collisions. *Comput. Phys. Commun.*, 100:128–156, 1997.
- [31] S. Jadach, B. F. L. Ward, and Z. Was. The precision monte carlo event generator kk for two- fermion final states in e^+e^- collisions. *Comput. Phys. Commun.*, 130:260, 2000.
- [32] Torbjorn Sjostrand. PYTHIA 5.7 and JETSET 7.4: Physics and manual. 1995.
- [33] G. Altarelli and G. Parisi. Asymptotic freedom in parton language. *Nucl. Phys.*, B126:298, 1977.
- [34] G. Altarelli et al. *Physics at LEP2*. Cern Geneva, 1996.
- [35] G. Abbiendi et. al. The OPAL Collaboration. Model independent searches for scalar bosons with the OPAL detector at LEP. OPAL Physics Note PN449, 2000.
- [36] The OPAL Collaboration. The OPAL detector at LEP. *Nuclear Instrumentation and Methods A*, page 275, 1991.
- [37] S. Mihara and S. Yamashita. MT 3.00 – a new algorithm to calculate energy flows based on the MT package. OPAL Technical Note TN 575, 1998.
- [38] Satoru Yamashita. personal communication.
- [39] Satoru Yamashita. Attempt to develop new jet-particle association methods for a four-jet topology with the opal detector. OPAL Technical Note TN579, 1998.
- [40] S. Catani et. al. New clustering algorithm for multijet cross sections in e^+e^- annihilation. *Physics Letters B*, page 432, 1991.
- [41] S. Bethke et. al. New jet cluster algorithms: Next-to-leading order QCD and hadronization corrections. *Nuclear Physics B*, page 310, 1992.
- [42] S. Bethke et. al. JADE Collaboration. Experimental investigation of the energy dependence of the strong coupling strength. *Physics Letters B*, page 235, 1988.
- [43] K. Ishii, T. Saeki, and S. Yamashita. Jet error parametrisation. OPAL Technical Note TN449, 1996.
- [44] F.A. Berends, R. Pittau, and R. Kleiss. Excalibur, a monte carlo program to evaluate all four-fermion processes at LEP 200 and beyond. *Computer Physics Communications*, page 437, 1995.

- [45] J. Böhme. *Suche nach assoziierter Produktion von Higgs- und Z^0 -Bosonen mit Zerfall in Quarks oder Gluonen am OPAL-Experiment.* PhD thesis, Rheinisch-Westfälische Technische Hochschule Aachen, 2000.
- [46] J. Böhme. Implementation of the higgs-strahlung matrix element. OPAL Technical Note TN607, 1999.
- [47] The OPAL Collaboration. Search for neutral higgs bosons in e^+e^- collisions at $\sqrt{s} \sim 189$ GeV. *European Physical Journal* **C12**, page 567, 2000.
- [48] G. Parisi. Superinclusive cross sections. *Physics Letters*, page 65, 1978.
- [49] J. F. Donoghue, F. E. Low, and So-Young Pi. Tensor analysis of hadronic jets in quantum chromodynamics. *Physical Review D*, page 2759, 1979.
- [50] S. Catani and B. R. Webber. Resummed c-parameter distribution in e^+e^- annihilation. *Physics Letters B*, page 377, 1998.
- [51] Benno List. Figure of merit. OPAL Technical Note 619, 1999.
- [52] K. Desch, L. Feld, T. Kuhl, M. Schumacher, E. v. Toerne, and N. Wermes. Search for standard model higgs in the 4-jet channel at $\sqrt{s} = 170(2)$ GeV with a likelihood method. OPAL technical note TN488, 1997.
- [53] M. Schuhmacher. *Suche nach neutralen Higgs-Bosonen mit dem OPAL-Detektor bei LEP2.* PhD thesis, Universität Bonn, 1999.
- [54] P. Bock. Determination of exclusion limits for particle production using different decay channels with different efficiencies, mass resolutions, and backgrounds. to be submitted to Nucl. Inst. and Meth., 1996.
- [55] F. James, L. Lyons, and Y. Perrin, editors. *Workshop on Confidence Limits*, 2000. CERN 2000-005.
- [56] G. Abbiendi et. al. The OPAL Collaboration. Searches for higgs bosons in extensions to the standard model in e^+e^- collisions at the highest LEP energies. OPAL Physics Note PN472, 2001.
- [57] Xavier Calmet. personal communication.

Acknowledgements

Doing this thesis meant a year full of work and of fun. Of course I would not have been able to do it without the help of many people. And I had even more than one "rescue team" by my side.

First of all the "Munich team", especially *Thomas Trefzger* and *Madjid Boutemour*, who helped me out of quite a number of smaller (and bigger) emergencies, and Thomas even from quite a number of different corners on this planet!

Some of the beginner's hurdles were further lowered by *Tatjana Unverhau* and *Tim Christiansen*. Thanks to *Xavier Calmet* for extra branching fractions and all the other theoretical "advices"! Special thanks of course to *Dorothee Schaile*, that she made it possible for me to stay at CERN and to work directly with the OPAL Higgs Hunters

... who formed my "Geneva rescue team", most of all *Fredrik Akesson*, *Tom Junk*, *Arnulf Quadt* and *Satoru Yamashita*. They were quite a bit completed by the "Hamburg rescue team", namely *Jenny Böhme* and *Götz Gaycken*.

Rescue was not only necessary *with* work but also *from* work. This job was wonderfully done by *Filip*, *Asia*, *Barbara*, *Blandine*, *Bernardo*, *Evelyne*, *Frank*, *Georg*, *Giovanna*, *Jesse*, *Joana*, *Marco*, *Michael*, *Olivier*, *Pablo*, *Peter*, *Peter*, *Sue* and *Vincent*.

James Letts was the one rescuer who managed to save me both with work and from it, by solving numerous computer problems, checking thoroughly each page of this thesis, providing a spare desk and computer, bringing coffee to my desk when necessary – and most of all by being a true friend.

Erklärung

Ich versichere hiermit, die vorliegende Arbeit selbständig verfasst zu haben und keine anderen als die angegebenen Quellen und Hilfsmittel benutzt zu haben.

München, den 15. Mai 2001

Nicole Nesvadba

